

The FTS-Hook-FHIP (FHF) complex interacts with AP-4 to mediate perinuclear distribution of AP-4 and its cargo ATG9A

Rafael Mattera^a, Chad D. Williamson^a, Xuefeng Ren^b, and Juan S. Bonifacino^{a,*}

^aNeurosciences and Cellular and Structural Biology Division, Eunice Kennedy Shriver National Institute of Child Health and Human Development, National Institutes of Health, Bethesda, MD 20892; ^bDepartment of Molecular and Cell Biology and California Institute of Quantitative Biosciences, University of California, Berkeley, Berkeley, CA 94720

ABSTRACT The heterotetrameric adaptor protein complex 4 (AP-4) is a component of a protein coat associated with the *trans*-Golgi network (TGN). Mutations in AP-4 subunits cause a complicated form of autosomal-recessive hereditary spastic paraplegia termed AP-4-deficiency syndrome. Recent studies showed that AP-4 mediates export of the transmembrane autophagy protein ATG9A from the TGN to preautophagosomal structures. To identify additional proteins that cooperate with AP-4 in ATG9A trafficking, we performed affinity purification-mass spectrometry followed by validation of the hits by biochemical and functional analyses. This approach resulted in the identification of the fused toes homolog-Hook-FHIP (FHF) complex as a novel AP-4 accessory factor. We found that the AP-4–FHF interaction is mediated by direct binding of the AP-4 μ 4 subunit to coiled-coil domains in the Hook1 and Hook2 subunits of FHF. Knockdown of FHF subunits resulted in dispersal of AP-4 and ATG9A from the perinuclear region of the cell, consistent with the previously demonstrated role of the FHF complex in coupling organelles to the microtubule (MT) retrograde motor dynein–dynactin. These findings thus uncover an additional mechanism for the distribution of ATG9A within cells and provide further evidence for a role of protein coats in coupling transport vesicles to MT motors.

Monitoring Editor

Adam Linstedt
Carnegie Mellon University

Received: Nov 25, 2019

Revised: Feb 5, 2020

Accepted: Feb 12, 2020

INTRODUCTION

The heterotetrameric adaptor protein (AP) complexes AP-1, AP-2, AP-3, AP-4, and AP-5 are components of protein coats involved in the sorting of transmembrane protein cargo in post-Golgi compartments of the endomembrane system of eukaryotic cells (reviewed

by Robinson 2015; Guardia *et al.*, 2018). These complexes are composed of two large subunits ($\gamma/\alpha/\delta/\epsilon/\zeta$ and $\beta 1/\beta 2/\beta 3/\beta 4/\beta 5$), a medium-sized subunit ($\mu 1/\mu 2/\mu 3/\mu 4/\mu 5$), and a small subunit ($\sigma 1/\sigma 2/\sigma 3/\sigma 4/\sigma 5$) (Robinson, 2004; Guardia *et al.*, 2018). The composition of AP complexes is further diversified by the existence of paralogous isoforms of the γ , $\mu 1$, $\sigma 1$, α , $\beta 3$, $\mu 3$, and $\sigma 3$ subunits (Mattera *et al.*, 2011). Each AP complex consists of a core formed by the medium and small subunits together with the N-terminal “trunk” domains of the large subunits; extending from this core are the two C-terminal “hinge” and “ear” domains of the large subunits (see Figure 1A for a scheme of AP-4). Each AP complex has a different localization within the cell: AP-1 is found at the *trans*-Golgi network (TGN) and endosomes, AP-2 at the plasma membrane, AP-3 on a tubular endosomal compartment, AP-4 at the TGN, and AP-5 at late endosomes (Robinson, 2004; Guardia *et al.*, 2018). The complexes are recruited to membranes by interactions with small GTPases of the ARF family and/or membrane phosphoinositides, and associate with scaffolding and accessory proteins, resulting in the assembly of protein coats (Robinson, 2004; Guardia *et al.*, 2018). APs then

This article was published online ahead of print in MBoc in Press (<http://www.molbiolcell.org/cgi/doi/10.1091/mbc.E19-11-0658>) on February 19, 2020.

*Address correspondence to: Juan S. Bonifacino (juan.bonifacino@nih.gov).

Abbreviations used: AD, activation domain; AP, adaptor protein; AT, 3-amino-1,2,4 triazole; CT, threshold cycle; FHF, FTS-Hook-FHIP; FHIP, FTS and Hook-interacting protein; FTS, fused toes homolog; HD, Hook domain; IB, immunoblot; IF, immunofluorescence; IP, immunoprecipitation; KD, knockdown; LIC, light intermediate chain; MS, mass spectrometry; MT, microtubule; PBS, phosphate-buffered saline; TAP, tandem affinity purification; TGN, *trans*-Golgi network; TSF, two-Strep/one-FLAG; μ HD, μ homology domains; Y2H, yeast two-hybrid.

© 2020 Mattera *et al.* This article is distributed by The American Society for Cell Biology under license from the author(s). Two months after publication it is available to the public under an Attribution–Noncommercial–Share Alike 3.0 Unported Creative Commons License (<http://creativecommons.org/licenses/by-nc-sa/3.0>).

“ASCB®,” “The American Society for Cell Biology®,” and “Molecular Biology of the Cell®” are registered trademarks of The American Society for Cell Biology.

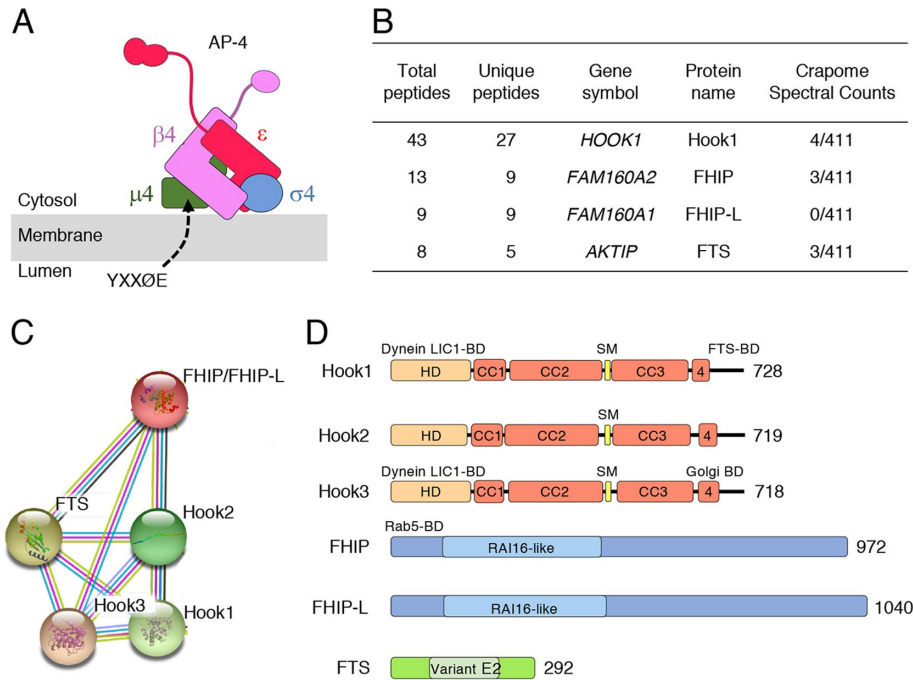


FIGURE 1: TAP-MS identifies the FHF complex as an AP-4 interactor. (A) Schematic representation of the AP-4 heterotetramer depicting the ϵ , $\beta 4$, $\mu 4$, and $\sigma 4$ subunits. The hinge and ear domains of ϵ and $\beta 4$ are shown protruding from their corresponding trunk domains. Two subdomains, an N-terminal β sandwich, and a C-terminal platform are predicted for the ϵ ear domain while a single C-terminal platform is predicted for the $\beta 4$ ear (Mattera et al., 2011, 2015). Also shown is the YXXØE sequence motif in transmembrane cargo proteins such as the amyloid precursor protein and ATG9A that is recognized by the AP-4 $\mu 4$ subunit (Burgos et al., 2010; Mattera et al., 2017). (B) TAP-MS analysis of proteins copurifying with two-Strep/one FLAG (TSF)-tagged AP-4 ϵ expressed in stably transfected H4 human neuroglioma cells identifies subunits of the FHF complex as AP-4 interactors. The FHF subunits identified by MS are ranked by the number of total and unique peptides and scored according to the contaminant repository for affinity purification (CRAPome) database (www.crapome.org) (see Dataset S1 in Mattera et al., 2017). (C) Interaction cluster of the FHF complex subunits obtained from the String website (www.string-db.org). Subunits in the cluster include Hook1, Hook2, Hook3, FHIP (encoded by the *FAM160A2* gene), and FTS (also termed AKT-interacting protein, AKTIP). Interactions with other proteins that are not part of the FHF complex have been removed for simplicity. The product of the *FAM160A1* gene displaying 36.5% identity and 63.3% similarity with FHIP (herein referred to as FHIP-like or FHIP-L) was also identified as an AP-4-interacting protein in our TAP/MS analysis (B). This protein is listed as a potential interactor for both Hook3 and FTS in the BioGRID database (www.thebiogrid.org) based on BioPlex 2.0 affinity capture-MS analysis (Huttlin et al., 2017). (D) Schematic representation of components of the human FHF complex including Hook1, Hook2, Hook3, FHIP (two isoforms containing 986 and 972 residues have been described; the shortest form is depicted here), FHIP-L, and FTS. The domains highlighted in Hook proteins include the HD involved in recognition of the dynein LIC1 by Hook1 and Hook3, the predicted coiled-coil regions (CC1-4; CC4 is abbreviated as “4”), the Spindly like motif (SM), the FTS-BD (residues 657–728) in Hook1, and the Golgi BD (residues 589–718) in Hook3 (Walenta et al., 2001; Xu et al., 2008, Schroeder and Vale 2016; Gama et al., 2017, Lee et al., 2018). Highlighted in FHIP and FHIP-L are the retinoic acid-induced 16-like protein (RAI16-like) domain (EMBL-EBI InterPro number IPRO019384) and the Rab5-BD in FHIP (residues 1–426, Guo et al., 2016). Highlighted in FTS is the variant ubiquitin-conjugating enzyme domain (variant E2, also termed UEV) (Hurley et al., 2006).

function to recognize signals in the cytosolic tails of transmembrane protein cargos leading to the incorporation of the cargos into transport carriers (Traub and Bonifacino, 2013).

The AP-4 complex (Figure 1A) was independently identified two decades ago by our laboratory (Dell’Angelica et al., 1999) and that of Margaret S. Robinson (Hirst et al., 1999). AP-4 was found to be present in a wide variety of eukaryotes, although not in the genetic

model organisms *Saccharomyces cerevisiae*, *Drosophila melanogaster*, and *Caenorhabditis elegans*, probably due to gene loss during evolution (Hirst et al., 2014). Studies using mammalian cells showed that AP-4 associates with the TGN by virtue of interactions with ARF GTPases, and that it does not interact with the scaffolding protein clathrin (Dell’Angelica et al. 1999; Hirst et al. 1999; Boehm et al., 2001). At present it is unclear whether or not AP-4 interacts with a nonclathrin scaffold. Subsequent studies revealed that the $\mu 4$ subunit of AP-4 preferentially recognizes sorting signals fitting the consensus motif YXXØE (where X is any amino acid and Ø is a bulky hydrophobic amino acid) (Burgos et al., 2010; Mattera et al., 2017), as well as noncanonical sequences (Yap et al., 2003). AP-4 has been the focus of renewed attention in recent years due to the finding that mutations in each of its subunits are the cause of a subset of autosomal-recessive hereditary spastic paraplegia (abbreviated HSP or SPG) types characterized by progressive spasticity and intellectual disability. This subset, referred to as “AP-4-deficiency syndrome,” comprises SPG47 (AP4B1, $\beta 4$), SPG50 (AP4M1, $\mu 4$), SPG51 (AP4E1, ϵ), and SPG52 (AP4S1, $\sigma 4$) (mutated gene and protein subunit are indicated in parentheses; Verkerk et al., 2009; Abou Jamra et al., 2011; Moreno-De-Luca et al., 2011; for a review, see Tesson et al., 2015). The link of AP-4 to a human disease spurred further efforts to identify additional interactors and elucidate the molecular basis for the disease. Affinity purification and mass spectrometry (MS) analyses led to the identification of the accessory proteins tepisin (Borner et al., 2012; Mattera et al., 2015; Frazier et al., 2016), RUSC1 and RUSC2 (Davies et al., 2018), and the transmembrane protein cargos ATG9A (Mattera et al., 2015, 2017; Davies et al., 2018; Ivankovic et al., 2020), SERINC1, and SERINC3 (Davies et al., 2018) as relevant AP-4 interactors. Mutations in AP-4 were shown to result in defective transport of ATG9A, SERINC1, and SERINC3 from the TGN to the cell periphery (Mattera et al., 2017; Davies et al., 2018, De Pace et al., 2018; Ivankovic et al., 2020), indicating that AP-4 plays a role in protein export from the TGN.

The finding that ATG9A is an AP-4 cargo was particularly relevant because ATG9A is a critical component of the autophagy machinery, which contributes to the formation and expansion of preautophagosomal structures. ATG9A mutations in mice are associated with axonal dystrophy and a thin corpus callosum (Yamaguchi et al., 2018), as is also the case for mice with mutations in AP-4 subunits (De Pace et al., 2018; Ivankovic et al., 2020) and human patients with AP-4-deficiency syndrome (Verkerk et al., 2009; Moreno-De-Luca et al., 2011;

Bauer *et al.*, 2012; Tüysüz *et al.*, 2014; Abdollahpour *et al.*, 2015; Hardies *et al.*, 2015; Ebrahimi-Fakhari *et al.*, 2018). In accordance with the role of AP-4 in TGN export of ATG9A, AP-4-deficient mice and humans were found to exhibit defects in autophagy, suggesting that impaired autophagy contributes to the pathogenesis of this disorder. Despite this progress in the understanding of AP-4 function, many aspects of its mechanism of action remain poorly understood.

To obtain additional insights into the physiological role of AP-4, we extended our analysis to other proteins that copurify with it in tandem affinity purification (TAP). Our results revealed that AP-4 specifically interacts with a multimeric complex termed FHF, which comprises the proteins “fused toes homolog” (FTS), Hook, and “FTS and Hook-interacting protein” (FHIP) (Krämer and Phistry, 1999; Walenta *et al.*, 2001; Xu *et al.*, 2008). In mammals, FTS is encoded by a single gene, whereas Hook exists as three paralogues named Hook1, Hook2, and Hook3, and FHIP as two paralogues named FHIP and FHIP-L. Components of this complex were previously shown to function as adaptors of organelles to dynein-dynactin and kinesin microtubule (MT) motors (Krämer and Phistry, 1999; Maldonado-Báez *et al.*, 2013; Bielska *et al.*, 2014; McKenney *et al.*, 2014; Zhang *et al.*, 2014; Xiang *et al.*, 2015; Guo *et al.*, 2016; Olenick *et al.*, 2016, 2019; Schroeder and Vale, 2016; Lee *et al.*, 2018; Urnavicius *et al.*, 2018; Dwivedi *et al.*, 2019a). In line with this function, we found that knockdown (KD) of FHF subunits causes dispersal of AP-4 and ATG9A from the perinuclear area of the cell, consistent with a defect in dynein-dynactin-dependent centripetal transport of AP-4 vesicles. Our findings thus extend the AP-4 interactome to a complex involved in the coupling of organelles to a retrograde transport motor.

RESULTS

Identification of the FHF complex as an AP-4 interactor

We previously reported the identification of proteins copurifying with the ϵ subunit of AP-4 (Figure 1A) in TAP-MS experiments (Mattera *et al.*, 2015; Dataset S1 in Mattera *et al.*, 2017). Whereas in earlier studies we focused on tepsin (Mattera *et al.*, 2015) and ATG9A (Mattera *et al.*, 2017; De Pace *et al.*, 2018), in this study we investigated four other copurifying proteins: Hook1 (product of the *HOOK1* gene), FHIP (FTS- and Hook-interacting protein) (product of the *FAM160A2* gene), the FHIP paralogue referred to in this study as FHIP-L (for FHIP-like) (product of the *FAM160A1* gene), and FTS (fused toes homolog) (product of the *AKTIP* gene) (Figure 1B). All of these proteins were identified with a relatively high peptide number, and had low scores (0/411 to 4/411) in the Contaminant Repository for Affinity Purification database (CRAPome, www.crapome.org; Mellacheruvu *et al.* 2013), suggesting that they were likely specific interactors. A similar TAP-MS analysis of proteins copurifying with the AP-4 accessory protein tepsin also yielded Hook1 as a high-ranking hit (Supplemental Table S1; see Supplementary Dataset S1 for a complete list of results). Hook1, FHIP, and FTS were previously shown to interact with each other as part of a complex named FHF, which may also include the Hook1 paralogues Hook2 and Hook3 (Xu *et al.*, 2008) (Figure 1, C and D). The status of FHIP-L vis-à-vis the FHF complex was not previously established.

To confirm the AP-4-FHF interaction, we transiently transfected HEK293T cells with plasmids encoding two-Strep/one-FLAG (TSF)-tagged forms of AP-4 ϵ or the myrlysin subunit of the BORC complex (Pu *et al.*, 2015) as a negative control. Pull down of cell lysates using StrepTactin beads followed by immunoblotting (IB) demonstrated the association of endogenous Hook1, Hook2, Hook3, and

FHIP with AP-4 ϵ but not the myrlysin control (Figure 2A). In addition, we performed immunoprecipitation (IP) from lysates of H4 human neuroglioma cells stably transfected with TSF-tagged AP-4 ϵ using anti-AP-4 β 4 or anti-GFP as a negative control. IB analysis revealed the co-IP of endogenous Hook1 and FHIP with antibody to endogenous AP-4 β 4 but not to GFP (Figure 2B). These experiments thus confirmed the interaction of AP-4 with subunits of the FHF complex.

AP-4-FHF interaction is mediated by AP-4 μ 4 and Hook proteins

We next used the yeast two-hybrid (Y2H) system to determine whether there is direct binding between AP-4 and FHF subunits. Interactions were detected by the ability of yeast expressing different combinations of AP-4 and FHF subunits fused to the Gal4-activation domain (AD) and Gal4-binding domain (BD) to grow on plates lacking histidine (-His) with varying concentrations of 3-amino-1,2,4 triazole (AT) to reduce background growth. The first set of assays (not including the FHIP-L paralogue) revealed interactions of the AP-4 μ 4 subunit with Hook1 and Hook2, but not Hook3, FHIP, and FTS (Figure 3A). Control experiments showed interactions of tepsin with AP-4 ϵ and AP-4 β 4, as previously reported (Borner *et al.*, 2012; Mattera *et al.*, 2015; Frazier *et al.*, 2016), and revealed an additional interaction of tepsin with AP-4 μ 4 (Figure 3A).

Further assays shown in Figure 3B demonstrated: 1) the ability of all Hook proteins to homodimerize, as previously shown for *Drosophila* Hook and mammalian Hook proteins (Krämer and Phistry 1996; Xu *et al.*, 2008; Lee *et al.*, 2018); b) the formation of Hook1-Hook3 heterodimers (Xu *et al.*, 2008); c) the binding of FHIP to Hook proteins (see also Supplemental Figure S1A); and d) the interaction of FTS with all the other subunits of the FHF complex.

To date, FHIP-L has not been shown to be a component of the FHF complex. Y2H analysis using a BD-FHIP-L construct showed nonspecific interactions even at high (30 mM) concentrations of AT (Supplemental Figure S1B). To circumvent this problem, we performed additional experiments with a reverse configuration using AD-FHIP-L and BD-AP-4 μ 4 constructs (Figure 3C). Using this configuration, we observed that FHIP-L binds to FTS and is therefore likely to be part of the FHF complex. Additionally, we found that, like FHIP (Figure 3A), FHIP-L does not interact with AP-4 μ 4 (Figure 3C). The BD-AP-4 μ 4 construct used in this configuration allowed us to confirm that AP-4 μ 4 directly binds to Hook1 and Hook2 (Figure 3C), as previously seen with the AD-AP-4 μ 4 construct (Figure 3A).

We also tested for interaction of Hook1 and Hook2 with μ subunits of other AP complexes. The results showed that Hook1 exclusively interacts with AP-4 μ 4, while Hook2 exhibits a broader pattern of interaction with AP-1 μ 1A and AP-2 μ 2, in addition to AP-4 μ 4 (Figure 3D). Additionally, we found that the interaction of AP-4 μ 4 with Hook1 and Hook2 is mediated by the C-terminal domain of AP-4 μ 4, which is also involved in the recognition of YXX ϕ E signals (Figure 3E) (Burgos *et al.*, 2010).

Taken together, these experiments demonstrated that AP-4-FHF interactions are mediated by the corresponding μ 4 and Hook1/ Hook2 subunits.

Mapping of Hook1 domains involved in interactions with AP-4 μ 4 and other FHF subunits

We also used the Y2H system to map the Hook protein domains involved in interactions with AP-4 μ 4 using Hook1 as a model protein (Figure 4A). Hook1 comprises a Hook domain (HD), four

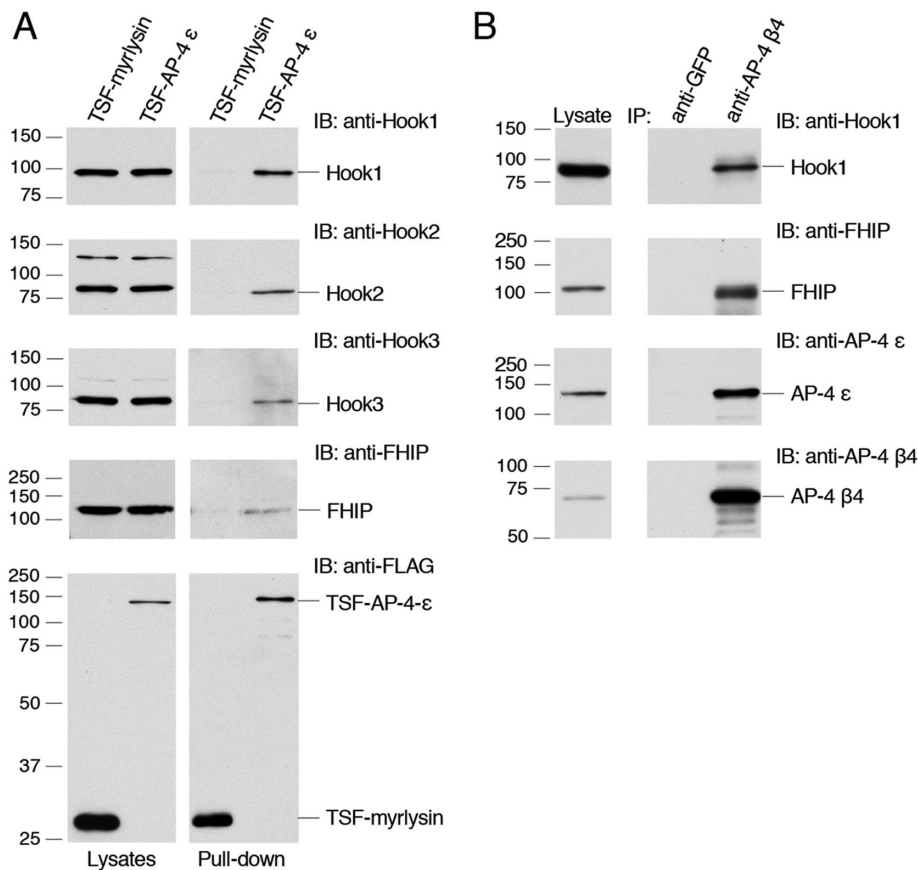


FIGURE 2: Pull down and co-IP experiments confirm the interaction of the FHF complex with AP-4. (A) HEK293T cells transiently transfected with TSF-tagged AP-4 ϵ or TSF-tagged myrlysin (one of the subunits of the BORC complex; Pu *et al.*, 2015) (negative control) were lysed and the cleared extracts were incubated with Strep-Tactin beads. Bound complexes and lysate samples (representing 0.4% of amount used for pull down) were subjected to SDS-PAGE and IB using antibodies to endogenous Hook proteins (Walenta *et al.*, 2001), FHIP or the FLAG epitope. (B) Lysates from H4 cells stably transfected with AP-4 ϵ were subjected to IP with either anti-AP-4 β 4 (Dell'Angelica *et al.*, 1999) or anti-GFP (negative control). Bound complexes and lysate samples (representing 1.5% of amount used for IP) were subjected to SDS-PAGE and IB with anti-Hook1, anti-FHIP, anti-AP-4 ϵ , and anti-AP-4 β 4 antibodies. Co-IP of Hook2 and Hook3 could not be evaluated due to the presence of nonspecific bands of similar mobility. The position of molecular mass markers (in kDa) is indicated at left of blots.

predicted coiled-coil regions (CC1–CC4; CC4 is abbreviated as “4” in the figure), a Spindly like motif (SM), and an FTS-BD (Walenta *et al.*, 2001; Xu *et al.*, 2008, Schroeder and Vale 2016; Gama *et al.*, 2017, Lee *et al.*, 2018) (Figure 4A). Analysis of various Hook1 deletion mutants (Figure 4A) showed that constructs having both the Hook1 CC1 and CC2 domains (constructs spanning residues 1–444, 1–658, 169–444, and 169–658) interacted with AP-4 μ 4 (Figure 4B). In contrast, the individual HD (1–168), CC1 (169–239), CC2 (240–444), or FTS-BD (658–728), or the CC3–CC4 combination (483–658) (Figure 4A) did not interact with AP-4 μ 4 in $-His +2$ mM AT plates, although weak interactions with constructs 1–239 and 658–728 could be detected in $-His$ plates without added AT (Figure 4B). Of note, the combination of the Hook1 CC1 and CC2 domains in the 1–444 and 169–444 constructs was also able to mediate Hook1 homodimerization and Hook1-Hook3 heterodimerization (Figure 4B). Thus, the first two coiled-coils in Hook1 are necessary and sufficient for interaction of Hook1 with AP-4 μ 4 as well as with Hook1 and Hook3. Interestingly, these coiled-coils are part of the region in Hook1 and Hook3 that is also important for

increasing both the affinity of dynein for dynactin and the processivity of the dynein–dynactin complex on binding of the HD to the dynein light intermediate chain (LIC) (Olenick *et al.*, 2016; Schroeder and Vale, 2016).

The experiments with deletion mutants also showed that the Hook 1 C-terminal region (658–728) binds not only FTS but also FHIP (Figure 4B). This suggested that FHIP assembles into the FHF complex through interactions with both FTS (Xu *et al.*, 2008) and Hook proteins. Further analyses of the interactions among Hook1, FHIP, and FTS showed that the quadruple mutation E661A, E662A, W669A, and Y670A in the C-terminal part of Hook1, previously shown to interfere with binding to FTS (Xu *et al.*, 2008), indeed prevented binding to FTS, but did not have any effect on interaction with AP-4 μ 4, Hook1 self-association or formation of Hook1-Hook3 heterodimers (Supplemental Figure S1C). Importantly, the Hook1 quadruple mutation did not affect binding to FHIP (Supplemental Figure S1C), indicating that different residues in the Hook1 C-terminal region are involved in interaction with FHIP and FTS. On the other hand, the FTS W106A-F107A double mutant (Xu *et al.*, 2008) abolished the interaction with Hook1, Hook2, and FHIP but had less of an effect on the interaction with Hook3 (Supplemental Figure S1D). These results suggest a different binding mode in the interaction of different Hook subunits with FTS, and that FTS W106A-F107A may not act as a complete dominant negative mutant of the FHF complex. A scheme depicting the domains involved in the interactions of Hook1 with AP-4 μ 4, FHIP and FTS, as well as in Hook1 self-association, is shown in Figure 4C.

Cellular distribution of Hook proteins and AP-4

The direct interaction between AP-4 and Hook1/Hook2 prompted us to analyze whether these proteins localized to the same subcellular compartments. To address this question, we used rabbit antisera to Hook1 and Hook2 developed in the Krämer laboratory (Walenta *et al.*, 2001). Although these antibodies, as well as the rabbit anti-Hook3 developed in the same lab, specifically recognized their antigens in IBs (Figure 5A), the anti-Hook2 antibody was the most specific for immunofluorescence (IF) microscopy. In agreement with previous reports (Baron Gaillard *et al.*, 2011; Dwivedi *et al.*, 2019a), IF microscopy with anti-Hook2 showed both perinuclear TGN and peripheral punctate staining (Figure 5C). This pattern was deemed specific, as it was markedly reduced in Hook2-KD cells (Figure 5D). Similar to the observations with anti-Hook2, the anti-AP-4 ϵ IF showed both perinuclear and peripheral staining in most cells (Figure 5C), which was reduced in the AP-4 ϵ KD cells (Figure 5E), as previously reported (Mattera *et al.*, 2017). Comparison of AP-4 ϵ and Hook2 immunostaining showed partial colocalization in the perinuclear region (Figure 5C). The perinuclear staining of

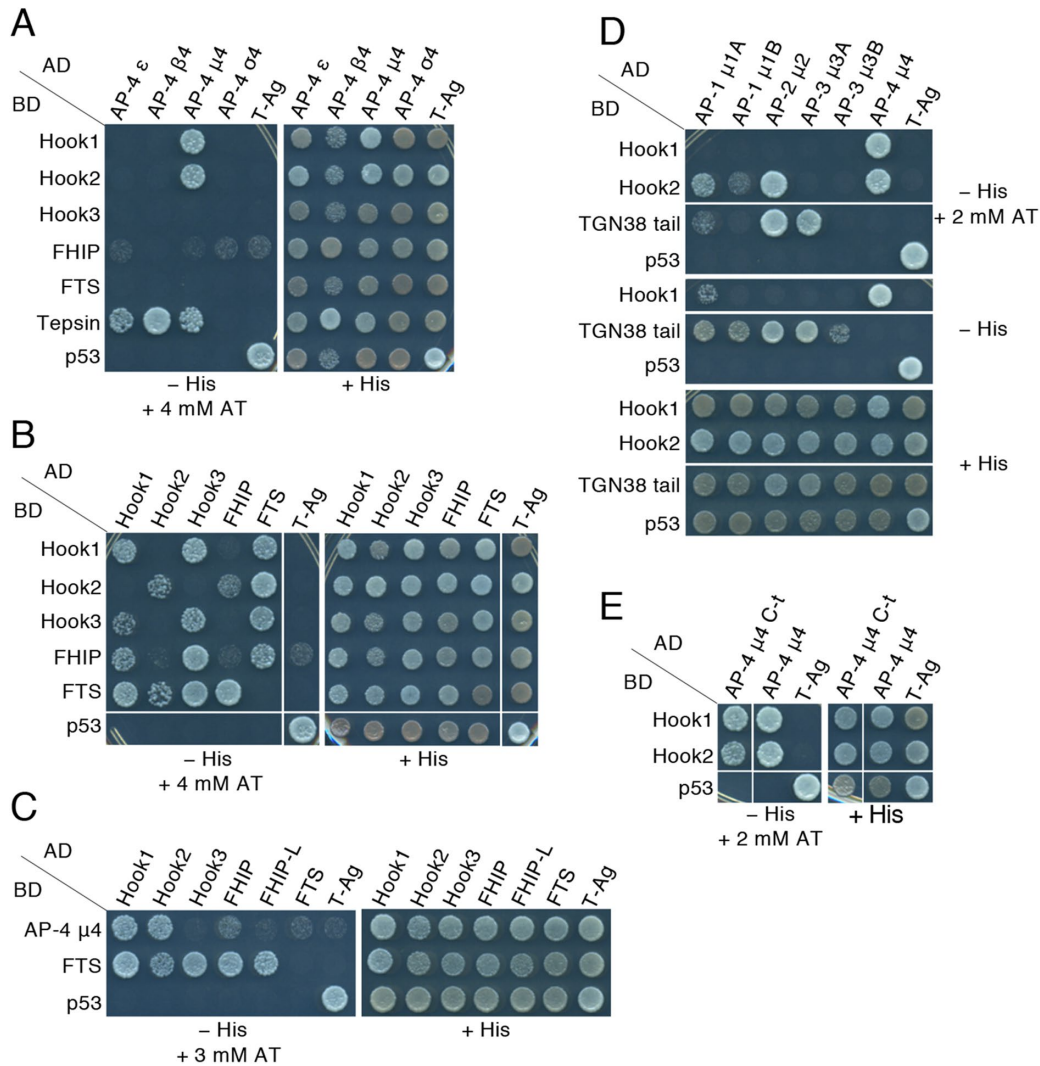


FIGURE 3: Y2H assays demonstrate direct interaction of AP-4 $\mu 4$ with Hook1 and Hook2, and reveal subunit interactions in the FHF complex. (A) Y2H analysis of interactions between subunits of the AP-4 and FHF complexes. Constructs were subcloned in Gal4 AD and Gal4 BD vectors, as indicated. Following double transformation of the AH109 yeast strain, the cotransformants were plated in medium containing histidine (+His) as control of growth/loading and in medium without histidine (-His) to assay for activation of the *HIS3* reporter gene on interaction of the constructs. The -His plates were supplemented with the indicated concentrations of AT, a competitive inhibitor of the His3 protein, to decrease background growth due to nonspecific interactions. Cotransformation of AD constructs with BD-p53 and of BD constructs with AD-SV40 large T antigen (T-Ag) provided negative controls, while double transformation with AD-T-Ag and BD-p53 was used as a positive control in the assays. The ϵ , $\beta 4$, $\mu 4$, and $\sigma 4$ constructs represent the different subunits of the AP-4 heterotetramer (Figure 1A). The results in the -His + 4 mM AT plate demonstrate the direct interaction of AP-4 $\mu 4$ with Hook1 and Hook2. In these experiments, we also used as control the AP-4 accessory protein tepsin which was previously shown to interact with both the ϵ and $\beta 4$ subunits of AP-4 (Borner *et al.*, 2012; Mattera *et al.*, 2015; Frazier *et al.*, 2016). We observed that the interaction of tepsin with AP-4 is actually trivalent, also involving direct binding to $\mu 4$ in addition to the ϵ and $\beta 4$ subunits of this adaptor complex. (B) Y2H analysis of the assembly of the FHF complex. The results in the -His + 4 mM AT plate show: 1) the homodimerization of all Hook proteins and the formation of Hook1-Hook3 heterodimers, 2) the interaction of FHIP with Hook proteins (interactions with different Hook proteins were identified in -His plates + 4 mM AT depending on whether the AD-FHIP or BD-FHIP construct was analyzed; see also Supplemental Figure S1A for similar assays in the absence of AT), and 3) the interaction of FTS with all other subunits of the FHF complex. (C) Analysis of FHIP-L interactions using AD-FHIP-L and BD-AP-4 $\mu 4$ constructs. Results show the interaction of the AD-FHIP-L construct with BD-FTS and also confirm the interaction of Hook1 and Hook2 with AP-4 $\mu 4$, as seen with constructs in the opposite configuration (A). (D) Interaction of Hook1 and Hook2 with μ subunits of different AP complexes. Hook1 exhibits selective interaction with AP-4 $\mu 4$, while Hook2 exhibits a broader pattern of interaction. The TGN38 cytosolic tail was used as a positive control for interaction with μ subunits of AP-1, AP-2, and AP-3 complexes (see -His plate). The interactions of Hook2 in -His plates are not shown because of nonspecific reporter gene activation observed with the BD-Hook2 construct in the absence of AT (see Supplemental Figure S1A). (E) Interaction of Hook1 and Hook2 with the C-terminal fragment of AP-4 $\mu 4$ (residues 91–453 in the human protein) which is also involved in recognition of tyrosine-based sorting signals. The images separated by thin lines in B, D, and E correspond to different areas of the same assay plates.

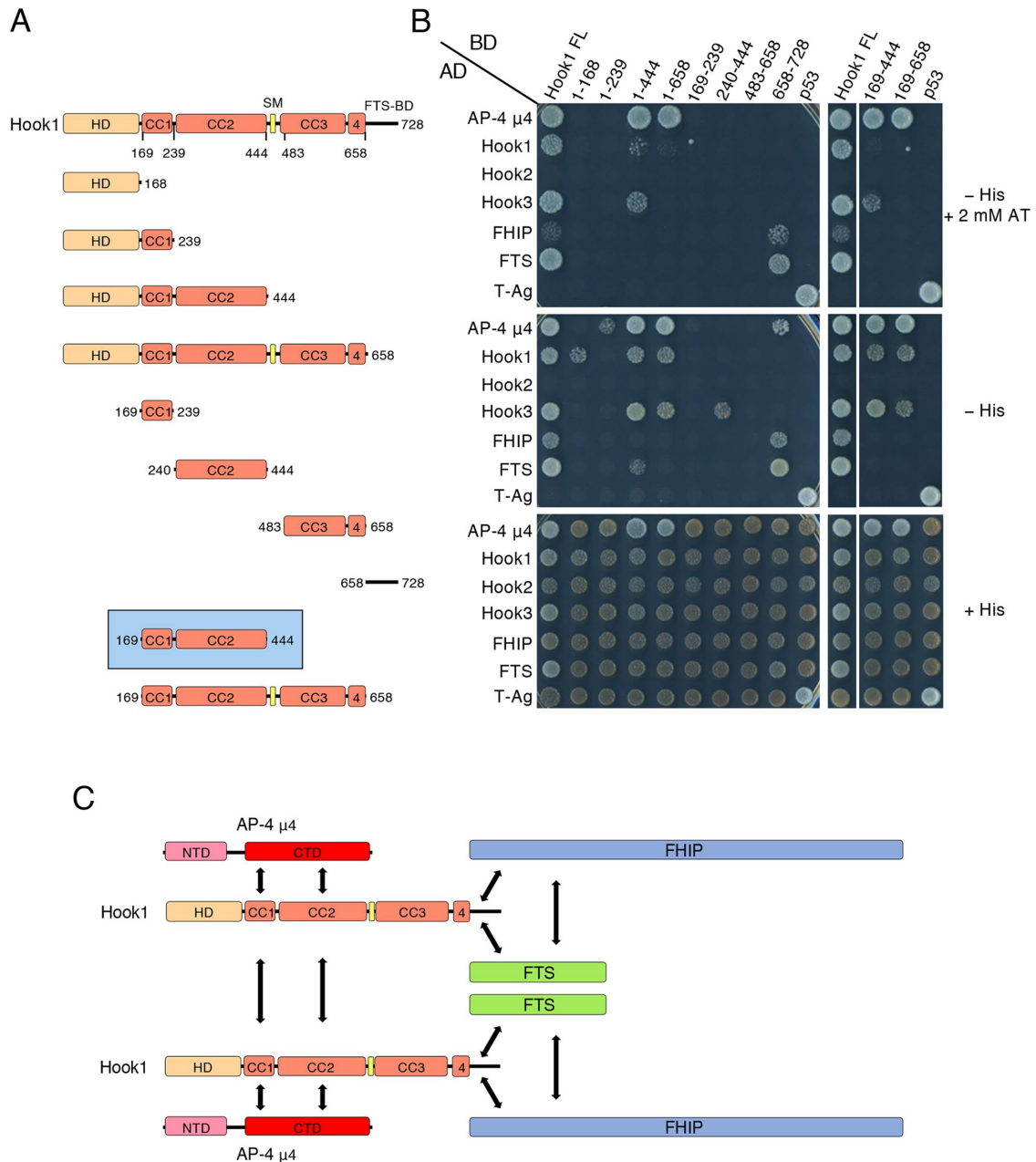


FIGURE 4: The Hook 1 CC1 and CC2 domains bind to AP-4 μ 4 and are required for Hook1 self-association and interaction with Hook3. (A) Scheme of the Hook1 constructs used in the Y2H analysis, as described in the legend to Figure 1D. The Hook1 minimal construct (including CC1 and CC2) is highlighted in blue. (B) Results of the Y2H analysis using different domains of Hook1 fused to Gal4 BD and full-length constructs of AP-4 μ 4, Hook1, Hook2, Hook3, FHIP, and FTS fused to Gal4 AD. Experiments were performed as described in the legend to Figure 3. The images separated by thin lines at the right of the panels correspond to different areas of the same assay plates. (C) Schematic representation of Hook1 interactions depicting self-association and binding to AP-4 μ 4 through CC1 and CC2 domains and binding to FHIP and FTS through its C-terminal region. Also shown is the direct interaction of FHIP with FTS. Different residues in the Hook1 C-terminal region are involved in recognition of FHIP and FTS (see Supplemental Figure S1C). The formation of Hook1-Hook3 heterodimers and the interaction of FTS with FHIP-L are not shown for simplicity. The AP-4 μ 4 N-terminal (α -helical) domain (NTD) involved in β 4 binding and the C-terminal (immunoglobulin-like β sandwich-folded) domain (CTD) involved in recognition of tyrosine-based signals are depicted in pink and red, respectively.

Hook2 was not affected by AP-4 ϵ silencing and vice versa (Figure 5, D and E), indicating that, although the AP-4 and FHF complexes interact and partially colocalize, they do not depend on each other for their localization. Given that AP-4 is expressed at very low levels, we also examined its colocalization with Hook2 in cells transfected

with expression vectors encoding all four subunits of AP-4. In transfected cells, we observed brighter AP-4 ϵ immunostaining in the TGN area compared with control cells, and this correlated with brighter immunostaining for Hook2 at the TGN (Figure 5F). The partial colocalization of Hook2 with AP-4 in the perinuclear area of the

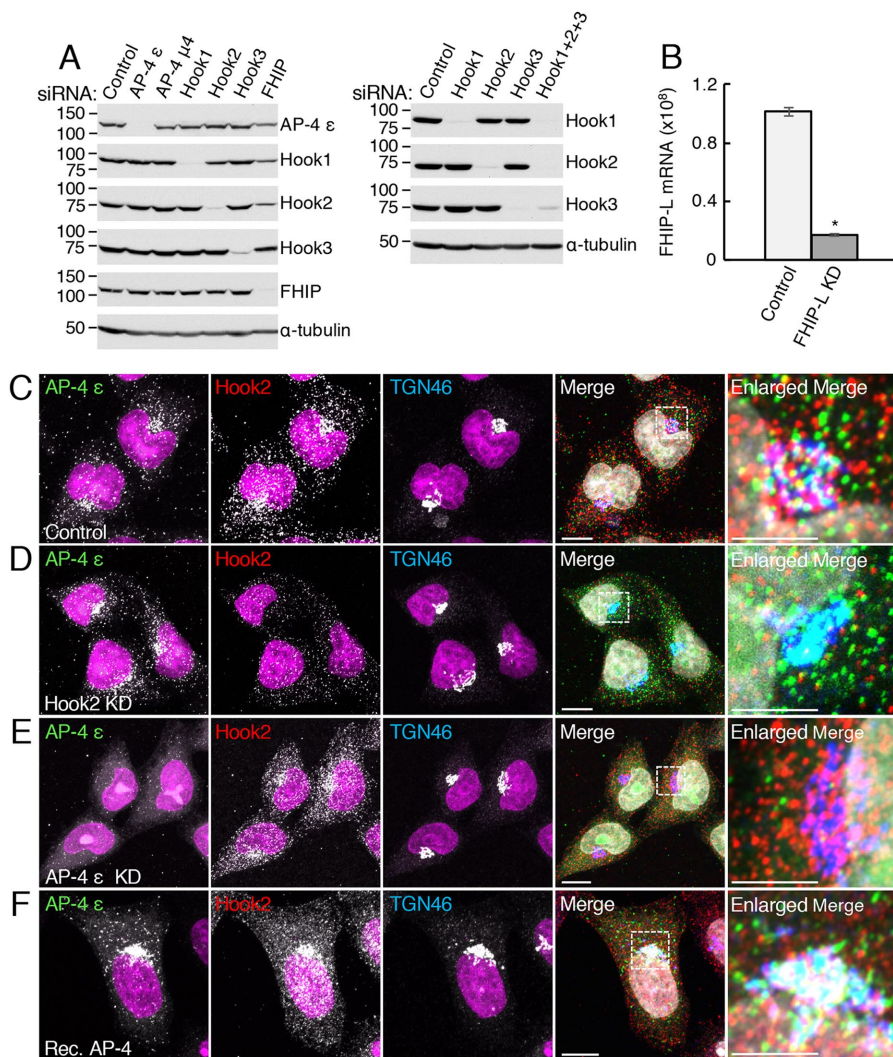


FIGURE 5: Distribution of AP-4 and Hook2 in HeLa cells. (A) IB analysis of HeLa cells treated with siRNA pools as described in *Materials and Methods*. Control cells were treated with a nontargeting siRNA. Cells were lysed and cleared extracts were subjected to SDS-PAGE and IB with the indicated antibodies. The position of molecular mass markers (in kDa) is indicated at left of blots. Results are representative of at least three independent experiments carried out with different batches of silenced cells prepared on separate days (usually weeks apart). (B) The efficiency of FHIP-L silencing was analyzed by quantitative real-time RT-PCR because of the unavailability of a specific anti-FHIP-L antibody. Results shown represent absolute cDNA levels arising from reverse transcription of 15 ng of total RNA (mean \pm SD of technical triplicates; $*P < 10^{-6}$, unpaired one-tailed Student's *t* test). The mRNA expression in FHIP-L-silenced samples relative to HeLa cells treated with nontargeted siRNA (Control) and normalized using β -actin as reference gene was 0.199. (C–E) Control, Hook2-, and AP-4 ϵ -siRNA-treated HeLa cells were immunostained for endogenous AP-4 ϵ , Hook2, and TGN46 and imaged by confocal fluorescence microscope. (F) HeLa cells transfected with plasmids directing expression of all four AP-4 subunits (Rec. AP-4) were fixed, immunostained, and imaged as described for C–E. Single channel images in C–F are shown in inverted grayscale with DAPI staining of nuclei in magenta, while merged images depict staining of AP-4 ϵ , Hook2, and TGN46 in green, red, and blue, respectively, with nuclear staining in gray. Images in the last column are enlargements of the boxed areas in the merge panels. Although the antibodies to the different Hook proteins specifically recognized their antigens in IBs (A), the anti-Hook2 antibody was the most specific for IF microscopy analysis. The anti-Hook1 IF staining exhibited a perinuclear component in some cells together with small puncta scattered throughout the cytoplasm (possibly endosomes), along with an additional staining around the nuclear membrane that was also present in Hook1 KD cells (not shown). In contrast, immunostaining of Hook2 KD and AP-4 ϵ KD cells (D and E, respectively) demonstrated the specificity of anti-Hook2 and anti-AP-4 ϵ antibodies. Both AP-4 ϵ and Hook2 exhibited perinuclear and peripheral immunostaining (see C and F for staining of

cells is consistent with the interaction of AP-4 with FHF occurring at this location.

KD of FHF complex subunits causes redistribution of AP-4 and ATG9A toward the cell periphery

Our observation of direct binding and partial colocalization of the AP-4 and FHF prompted us to analyze a possible functional relationship of these complexes. In view of the binding of Hook proteins to the dynein LIC and, possibly, to dynactin subunits, and of their effects on dynein–dynactin processivity (Schroeder and Vale, 2016; Lee *et al.*, 2018; Qiu *et al.*, 2018; Urnavicius *et al.*, 2018; Dwivedi *et al.*, 2019a), we investigated the effect of siRNA-mediated down-regulation of FHF subunits on the localization of AP-4 and its cargo ATG9A (Mattera *et al.*, 2017; Davies *et al.*, 2018; De Pace *et al.*, 2018; Ivankovic *et al.*, 2020). Due to a possible redundancy in the function of Hook proteins, we tested the effects of the combined KD of Hook1, Hook2, and Hook3 subunits. We also tested the individual KD of FHIP and FHIP-L. IB analysis showed that cells subjected to two rounds of treatment with siRNAs exhibited efficient silencing of their corresponding targets (Figure 5A). Silencing of FHIP-L could not be evaluated by IB due to the unavailability of specific antibodies to this protein and was therefore confirmed by quantitative real-time RT-PCR (Figure 5B). In these experiments, we included two additional conditions as controls. First, we examined changes in the distribution of AP-4 and ATG9A on overexpression of the GFP-labeled CC1 domain of the p150^{Glued} dynactin subunit (GFP-p150-CC1), which is known to disassemble the endogenous dynein–dynactin complex and to prevent dynein–dynactin-dependent retrograde transport (Quintyne *et al.*, 1999). Second, we examined the effect of AP-4 μ 4 KD on the distribution of ATG9A, which requires AP-4 for export from the TGN (Mattera *et al.*, 2017; Davies *et al.*, 2018; De Pace *et al.*, 2018; Ivankovic *et al.*, 2020). We observed that overexpression of GFP-p150-CC1 resulted in marked dispersal of both AP-4 (Figure 6, A and B) and ATG9A (Figure 7, A and B) from the perinuclear area in virtually all cells (see quantification in Figure 8A), whereas AP-4 μ 4 KD caused increased accumulation of

endogenous and recombinant AP-4 ϵ , respectively). Images shown are multiple intensity projections prepared from Z-stacks. Scale bars: 5 μ m for enlarged images (right column) and 10 μ m for all other images.

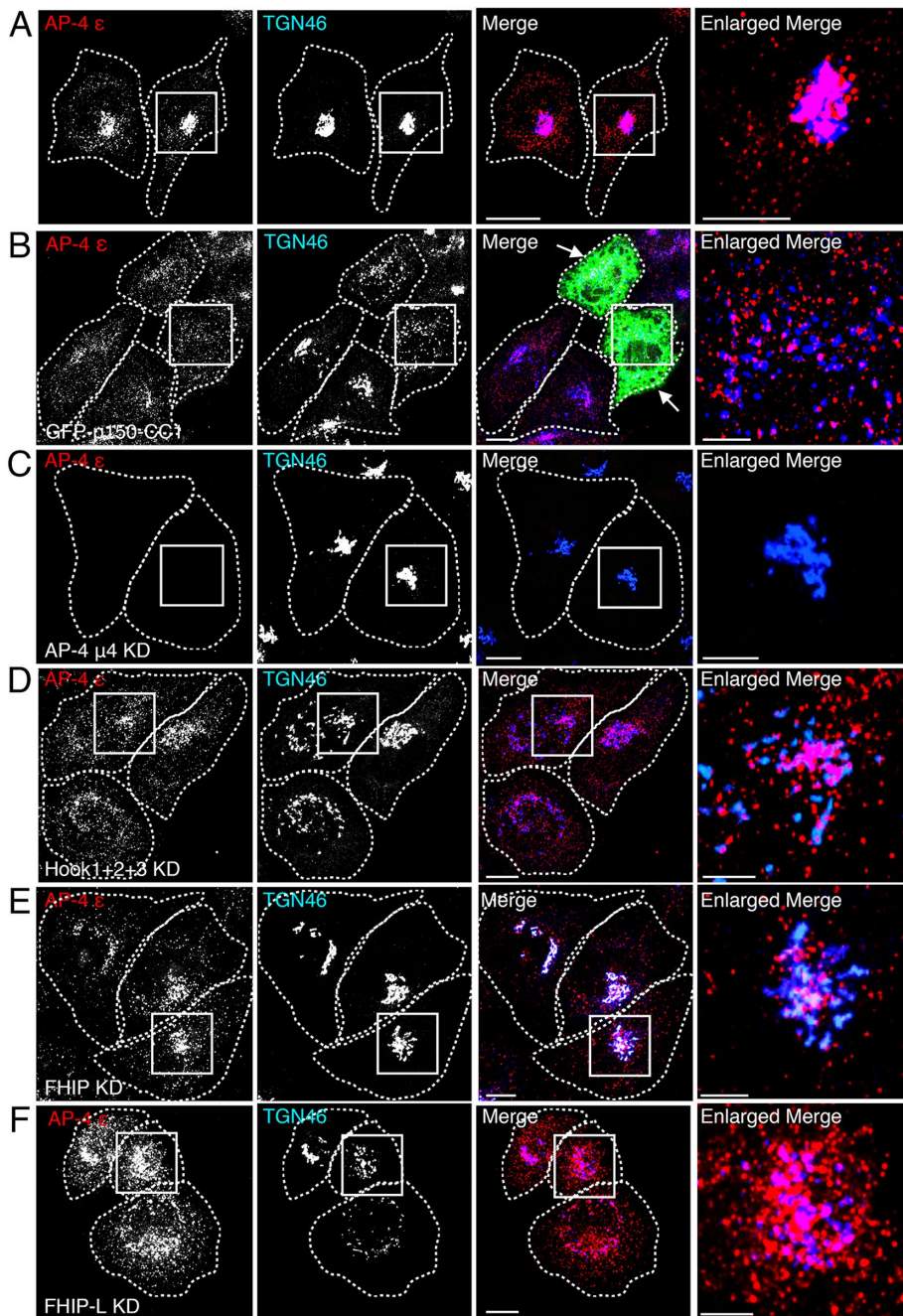


FIGURE 6: Distribution of AP-4 ϵ in HeLa cells with KD of FHF subunits. (A, C–F) HeLa cells were subjected to two rounds of treatment with the indicated siRNA pools as described in *Materials and Methods*. Cells were subsequently fixed with methanol at -20°C , coimmunostained for endogenous AP-4 ϵ and the TGN marker TGN46, and imaged by confocal microscopy. Single channel images are shown in inverted grayscale, whereas merge panels depict images of AP-4 ϵ and TGN46 in red and blue, respectively, with cells outlined by dashed white lines. Images in the right column are enlargements of the boxed areas. Panel A shows the predominantly perinuclear distribution of endogenous AP-4, while C represents a control experiment showing disappearance of this signal in AP-4 $\mu 4$ -silenced cells. Panels D–F show examples of AP-4 distribution in cells silenced for the indicated FHF subunits. Combined silencing of Hook1, Hook2, and Hook3 (Hook1+2+3 KD) (D), or of FHIP or FHIP-L (E and F, respectively) decreased the localization of AP-4 at the TGN in comparison to control cells (see Figure 8 for quantitative analysis). (B) Peripheral redistribution of AP-4 in cells transfected with a plasmid encoding the GFP-labeled CC1 domain of the p150^{Glued} dynein subunit (GFP-p150-CC1) known to cause disassembly of the dynein–dynactin complex (Quintyne *et al.*, 1999). Cells were fixed and coimmunostained for endogenous AP-4 ϵ and TGN46 (transfected cells were visualized with GFP-Booster Atto488). Single channel images of AP-4 ϵ and TGN46 are shown in

ATG9A at the TGN (Figure 7, A and C). These control experiments demonstrated our ability to observe changes in AP-4 and ATG9A distribution on specific perturbations. Importantly, although less pronounced than the effect of GFP-p150-CC1 overexpression, combined silencing of Hook1, Hook2, and Hook3 (Hook1+2+3), as well as individual silencing of FHIP or FHIP-L, caused dispersal of both AP-4 (Figure 6, D–F) and ATG9A from the TGN toward the peripheral cytoplasm (Figure 7, D–F) in 50–87% of the cells (Figure 8A).

Because overexpression of GFP-p150-CC1 or siRNA of FHF subunits also caused some dispersal of the TGN marker TGN46 (Figures 6 and 7), we quantified changes in the Spearman's r correlation coefficients for the colocalization of AP-4 or ATG9A with TGN46 (Figure 8, B and C). This quantification showed significant decreases in AP-4–TGN46 and ATG9A–TGN46 colocalization in GFP-p150-CC1-expressing cells (Figure 8, B and C) and a significant increase in ATG9A–TGN46 colocalization in AP-4 ϵ KD cells (Figure 8C). We also observed that KD of Hook1+2+3, FHIP, or FHIP-L resulted in significantly lower Spearman's correlation coefficients for the colocalization of AP-4 and ATG9A with TGN46 (Figure 8, B and C). Interference with dynein–dynactin or FHF subunits thus caused greater dispersal of AP-4 and ATG9A than of TGN46.

Taken together, these observations indicated that silencing of FHF subunits caused dispersal of AP-4 and ATG9A toward the cell periphery, most likely by impairing the coupling of vesicles containing these proteins to dynein–dynactin, with consequent inhibition of retrograde transport toward the central region of the cell.

Effect of KD of FHF complex subunits on autophagosomes

Because ATG9A is involved in the early stages of autophagosome formation and maturation, we examined whether the dispersal of ATG9A in FHF-depleted cells affected autophagy. To this end, we performed IB analysis to monitor the conversion of LC3B-I to LC3B-II, which is used

inverted grayscale with cells outlined by dashed white lines. Merge panel shows images of AP-4 ϵ , TGN46, and GFP-p150-CC1 in red, blue, and green, respectively, with the GFP-p150-CC1-transfected cells indicated by arrows. The right panel is an enlargement of the boxed area. Scale bars: 5 μm for enlarged images (right column) and 10 μm for all other images.

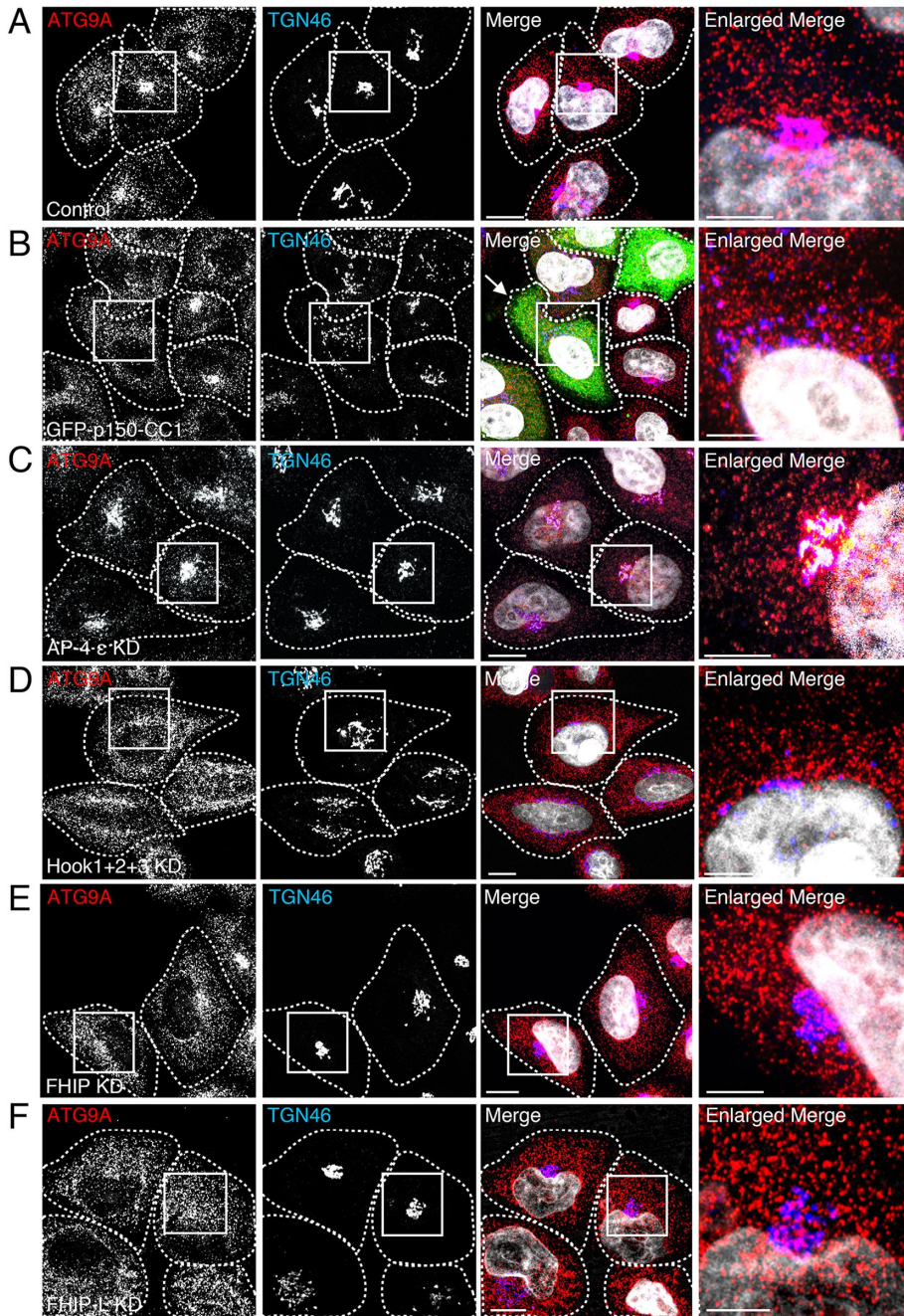


FIGURE 7: Distribution of ATG9A in HeLa cells with KD of FHF subunits. (A, C–F) HeLa cells were treated with the indicated siRNA pools and fixed as described in the legend to Figure 6. Cells were coimmunostained for ATG9A and the TGN marker TGN46 and imaged by confocal microscopy. Single channel images are shown in inverted grayscale, whereas merge panels depict images of ATG9A and TGN46 in red and blue, respectively, with DAPI staining of nuclei in gray (cells are outlined by dashed white lines). Images in the right column are enlargements of the boxed areas. Panel A displays the typical distribution of endogenous ATG9A between peripheral and perinuclear (i.e., TGN) compartments in control cells. Panel C represents a control experiment displaying increased accumulation of ATG9A at the TGN in AP-4-silenced cells in comparison to control cells (Mattera *et al.*, 2017; De Pace *et al.*, 2018; Davies *et al.* 2018; Ivankovic *et al.*, 2020). Silencing of FHF subunits including the combination of Hook1, Hook2, and Hook3 (Hook1+2+3 KD); or FHIP; or FHIP-L (D–F) decreased the localization of ATG9A at the TGN in comparison to control cells (see Figure 8 for quantification). (B) Redistribution of ATG9A to the peripheral cytoplasm in cells transfected with a plasmid encoding GFP-p150-CC1. Fixed cells were coimmunostained for ATG9A and TGN46 (transfected cells were visualized with GFP-Booster Atto488). Single channel images of ATG9A and TGN46 are shown in inverted grayscale with cells outlined by dashed white lines. The merge panel shows images of ATG9A,

as a reporter for autophagy (Kabeya *et al.*, 2004), in control cells versus cells subjected to either combined Hook1+2+3 silencing or individual silencing of FHIP or FHIP-L. These experiments showed no differences in the levels of the two LC3B species under both basal and starvation conditions, and also no difference in autophagic flux following inhibition of lysosomal degradation with bafilomycin A1 (Figure 9A). Likewise, IF microscopy showed no effect on the overall staining intensity of LC3B in control versus FHIP or FHIP-L KD cells (Figure 9, B–D). The only appreciable differences were alterations in the size and shape of LC3B-positive structures in a small percentage of FHF-deficient cells. In particular, we observed that ~3–7% of FHIP and FHIP-L KD cells exhibited LC3B-positive structures that were larger (0.9–1.6 μm diameter) than those in control cells (0.4–0.7 μm diameter) (Figure 9, B–D). In addition, we observed the appearance of tubular or “thread-like” LC3B-positive structures in ~4% of FHIP KD cells that were virtually absent in control cells (arrows in Figure 9C; see figure legend for quantification and statistical analysis). Thus, the dispersal of ATG9A in FHF-depleted cells was mostly inconsequential for autophagic flux, and only a small fraction of cells exhibited changes in autophagosome morphology.

DISCUSSION

Although the identification of ATG9A as an AP-4 cargo represented a significant advance in the understanding of AP-4 function (Mattera *et al.*, 2015, 2017; Davies *et al.*, 2018; De Pace *et al.*, 2018; Ivankovic *et al.*, 2020), a more complete picture of the AP-4 interactome is needed to fully explain the functional consequences of AP-4 deficiency. Our results contribute to this picture by revealing an interaction of AP-4 with the dynein–dynactin adaptor complex FHF and a role for the FHF complex in promoting the distribution of AP-4 and ATG9A to the perinuclear area of the cell.

Insights into the structure and function of the FHF complex

Xu *et al.* (2008) first demonstrated the existence of a complex termed FHF,

TGN46, and GFP-p150-CC1 in red, blue, and green, respectively, with the GFP-p150-CC1-transfected cells indicated by arrows. The right panel is an enlargement of the boxed area. Scale bars: 5 μm for enlarged images and 10 μm for all others.

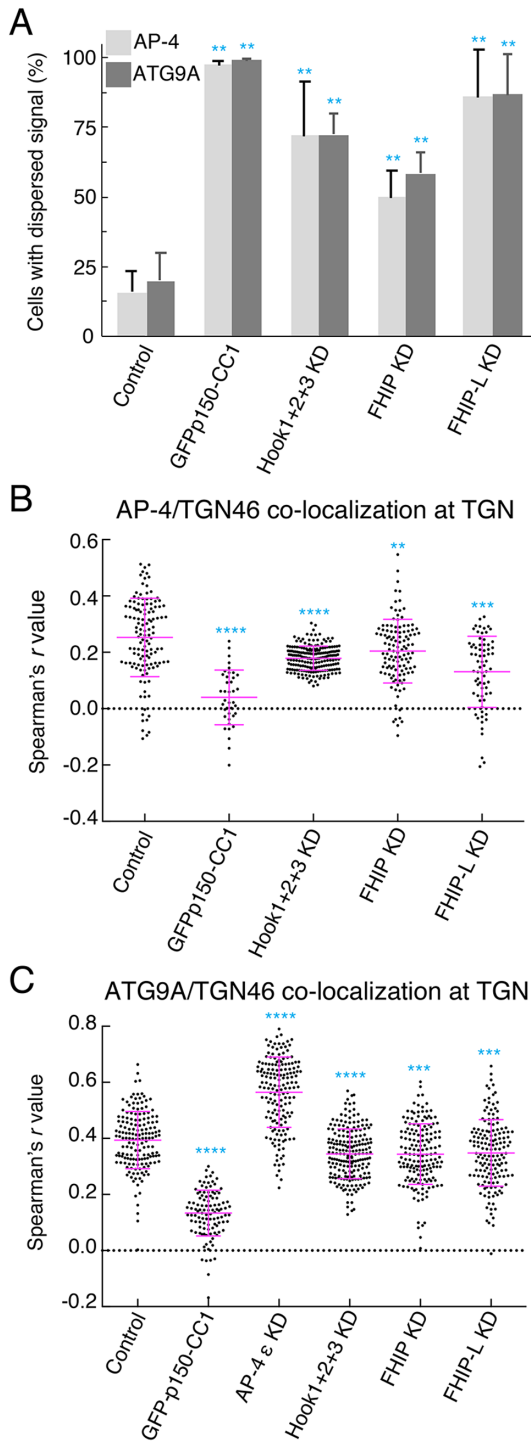


FIGURE 8: Quantification of the effects of FHF silencing on the cellular distribution of AP-4 and ATG9A. HeLa cells were treated with the indicated siRNA pools or transfected with a plasmid encoding GFP-p150-CC1, fixed, and immunostained for endogenous AP-4 ϵ , ATG9A, and the TGN marker TGN46 as described in the legends to Figure 6 and Figure 7. (A) Cells from two to four independent siRNA experiments were manually scored for dispersal of AP-4 or ATG9A from the perinuclear area. The number of cells scored was 2956 for AP-4 and 2736 for ATG9A in control cells, 421 for AP-4 and 476 for ATG9A in GFP-p150-CC1-transfected cells, 735 for both AP-4 and ATG9A in combined Hook1+2+3 KD cells, 619 for both AP-4 and ATG9A in FHIP KD cells, and 483 for both AP-4 and ATG9A in FHIP-L KD cells. Data shown are the mean \pm SD for each group. Statistical

composed of the previously identified FTS (Lesche *et al.*, 1997) and Hook proteins (Kramer and Phistry, 1999; Walenta *et al.*, 2001), and an additional component named FHIP. Early studies showed that Hook proteins mediate attachment of organelles to MTs (Walenta *et al.*, 2001) and participate in endosomal sorting of clathrin-independent cargo (Maldonado-Baez, 2013). Subsequent studies revealed that Hook proteins and other subunits of the FHF complex function as “activating adaptors” linking the MT motors dynein–dynactin (Bielska *et al.*, 2014; Yao *et al.*, 2014; Zhang *et al.*, 2014) and kinesin-3 (Bielska *et al.*, 2014) to early endosomes in filamentous fungi. Further studies showed that mammalian Hook1 and Hook3 induce longer and faster runs of dynein–dynactin on MTs (Olenick *et al.*, 2016; Schroeder and Vale 2016; Urnavicius *et al.*, 2018) and suggested a similar role for Hook2 (Dwivedi *et al.*, 2019a). These functional studies were extended to neurons with the demonstration that FHF complex subunits are required for dynein–dynactin-dependent retrograde axonal transport of Rab5- and transferrin-receptor-containing carriers (Guo *et al.*, 2016) and BDNF-signaling endosomes (Olenick *et al.*, 2019).

Recent structural studies shed light on the mechanistic bases for these functions of the FHF complex. The α -helical HD of Hook proteins was shown to bind to the C-terminal effector-BD of the dynein LIC (Schroeder and Vale, 2016; Lee *et al.*, 2018; Dwivedi *et al.*, 2019a). This binding as well as additional interactions with the Hook1 and Hook3 CC domains were found to be necessary for the processivity of dynein–dynactin (Olenick *et al.*, 2016; Schroeder and Vale, 2016). Recent studies also indicated that Hook3 can function as a scaffold for bidirectional cargo transport due to its direct binding to both dynein–dynactin and the kinesin-3 protein KIF1C (Kendrick *et al.*, 2019; Siddiqui *et al.*, 2019).

Whereas the FHF complex was initially thought to comprise Hook1-3, FTS and FHIP (Xu *et al.*, 2008), our TAP-MS and Y2H analyses, along with recent BioID-MS analysis of the dynein interactome (Redwine *et al.*, 2017), indicate that the product of the *FAM160A1* gene (herein referred to as FHIP-L) may also be part of this complex. Of note, a more distantly related gene product, *FAM160B1*, was also identified in the BioID-MS analysis of the Hook1 and Hook3 interactomes (Redwine *et al.*, 2017), suggesting that this protein could be a third alternative subunit of the FHF complex.

Our study also provides new insights into the assembly of the FHF complex. One aspect clarified by our Y2H analysis is the dimerization of Hook proteins. We observed that: 1) all Hook proteins homodimerize,

significance was analyzed by one-way ANOVA followed by two-tailed Dunnett’s test. $**P < 10^{-2}$ compared with control. (B) Colocalization of AP-4 and TGN46 distribution was analyzed through calculation of the Spearman’s rank correlation (r) (see *Materials and Methods*). The r value ranges from +1 to –1 for a perfectly positive to a perfectly negative correlation, with 0 denoting absence of correlation (dotted line parallel to the x-axis). Shown are the individual data points as well as the mean \pm SEM for each group. Results represent three independent siRNA experiments. The total number of cells analyzed was 127 (control), 39 (GFP-p150-CC1-transfected cells), 203 (combined Hook1+2+3 KD), 118 (FHIP KD), and 70 (FHIP-L KD). Statistical significance was analyzed by one-way ANOVA followed by two-tailed Dunnett’s test. $****P < 10^{-4}$; $***P < 10^{-3}$; $**P < 5 \times 10^{-3}$. (C) Quantification of changes in the colocalization of ATG9A and TGN46 at the TGN. Results were displayed and analyzed as described for B. The total number of cells analyzed was 163 (control), 108 (GFP-p150-CC1-transfected cells), 166 (AP-4 ϵ KD), 203 (combined Hook1+2+3 KD), 164 (FHIP KD), and 156 (FHIP-L KD). $****P < 10^{-4}$; $***P < 10^{-3}$.

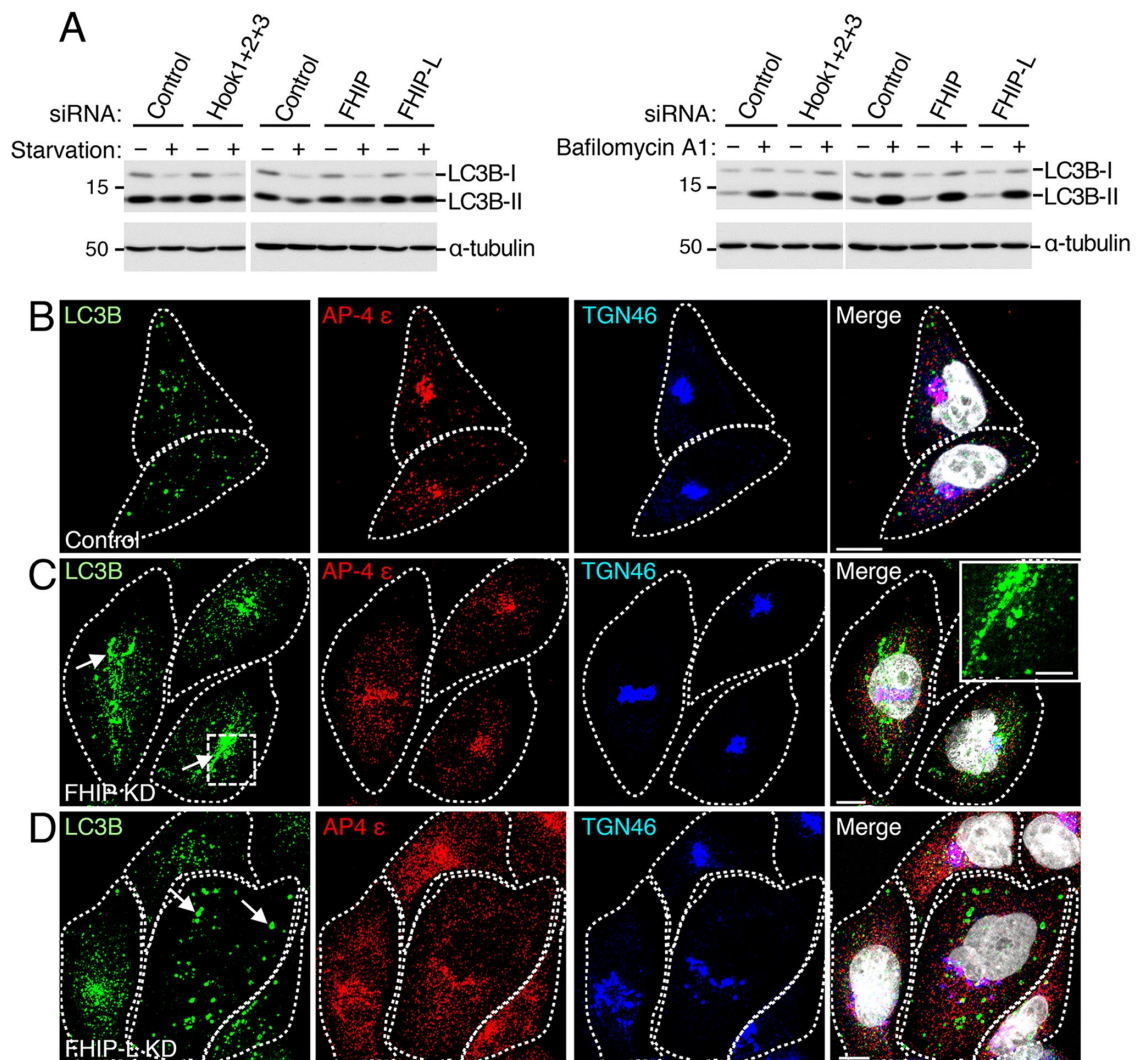


FIGURE 9: Conversion of LC3B-I to LC3B-II and morphology of autophagosomes in HeLa cells with KD of FHF subunits. HeLa cells were subjected to two rounds of treatment with the corresponding siRNA pools as described in *Materials and Methods*. (A) IB analysis of LC3B-I and LC3B-II in control and siRNA-treated cells seeded on 12-well plates and subjected to amino acid and serum starvation for 45 min at 37°C (image at left) or treatment with 100 nM bafilomycin A1 for 4 h at 37°C (image at right). IB for α -tubulin is shown as loading control. (B–D) Cells seeded on glass coverslips were fixed with methanol at –20°C and immunostained for endogenous LC3B, AP-4 ϵ , and TGN46 followed by confocal microscopy imaging. Anti-LC3B, anti-AP-4 ϵ , and anti-TGN46 immunostaining is shown in green, red, and blue, respectively. The panels at right depict merge images with DAPI staining of nuclei in gray (cells are outlined by dashed white lines). Arrows in C and D (left column) point at tubular or “thread-like” autophagosomes or large autophagosomes detected in a fraction of FHIP KD and FHIP-L KD cells, respectively (an enlargement of the area inside the white box in C is shown at the top right of the merge image). Scale bars: 5 μ m for the enlargement in C (right column) and 10 μ m for all other images. Cells were manually scored for the presence of LC3B-positive structures on threads or of large LC3B-positive structures (approximately 0.9–1.6 μ m diameter range). We observed that $4.3 \pm 0.7\%$ of FHIP KD cells exhibited autophagosomes on threads compared with $0.3 \pm 0.2\%$ in control cells and $0 \pm 0\%$ in FHIP-L KD cells (mean \pm SEM, $P < 10^{-2}$ for FHIP-L KD compared with control cells, one-way ANOVA followed by two-tailed Dunnett’s test). We also observed that $3.1 \pm 0.8\%$ and $7.1 \pm 0.8\%$ of FHIP KD and FHIP-L KD cells, respectively, exhibited large LC3B-positive structures compared with $0 \pm 0\%$ in control cells (mean \pm SEM; $P < 5 \times 10^{-2}$ for FHIP KD and $P < 10^{-2}$ for FHIP-L KD compared with control cells, one-way ANOVA followed by two-tailed Dunnett’s test). Values shown are from triplicate measurements including cells from two independent silencing experiments. Total number of cells analyzed in the three scorings was 1217 (control), 1373 (FHIP KD), and 481 (FHIP-L KD).

2) Hook1 and Hook3 heterodimerize, 3) Hook2 does not heterodimerize, and 4) the combination of the Hook1 CC1 and CC2 domains is necessary and sufficient for the formation of Hook1 homodimers and Hook1-Hook3 heterodimers. These results extend previous observations on the role of CC domains in the assembly of Hook protein complexes (Krämer and Phistry, 1996; Xu *et al.*, 2008; Lee *et al.*, 2018). A

second aspect highlighted by our experiments is that FHIP can bind directly to Hook proteins and is not just assembled into the FHF complex through its interaction with FTS (Xu *et al.*, 2008). We also demonstrated that the C-terminal region of Hook1 (residues 658–728) binds to both FHIP and FTS and that different residues in this region appear to be involved in recognition of FHIP and FTS.

Our observations on the predominant formation of Hook proteins homodimers and Hook1-Hook3 heterodimers, as opposed to heterodimers including Hook2, may have functional significance. Different Hook protein dimers could function at different cellular compartments as exemplified by the noninterchangeable roles of Hook paralogues during the initial stages of ciliogenesis (Baron Gaillard *et al.*, 2011) and mitotic progression and cytokinesis (Dwivedi *et al.*, 2019a). Alternatively, the differences in dimerization of Hook proteins could influence their function as dynein–dynactin adaptors. Each Hook protein dimer was initially assumed to bind two dynein LICs from a dynein dimer associated to a dynactin complex. However, recent cryo-electron microscopy and cryo-electron tomography structures, along with functional studies, revealed that Hook3 dimers favor the formation of complexes containing two dimeric dynein motors per dynactin, increasing the force and speed of the molecular motor (Grotjahn *et al.*, 2018; Urnavicius *et al.*, 2018; reviewed in Reck-Peterson *et al.*, 2018; Olenick and Holzbaur, 2019; and Dwivedi *et al.*, 2019b). It will now be of interest to compare the effects of Hook1, Hook2, and Hook3 homodimers, and of Hook1-Hook3 heterodimers, on the stoichiometry of dynein recruitment and processivity of dynein–dynactin complexes.

FHF as an AP-4 accessory protein complex

Our TAP-MS data along with the pull down and co-IP studies demonstrated an interaction between the AP-4 and the FHF complexes. Other recent proteomic analyses, including BioID-MS of the Hook1 interactome (Redwine *et al.*, 2017) and co-IP with GFP-tagged tepsin (Davies *et al.*, 2018), also pointed to a link between AP-4 and FHF. The Y2H analyses in the present study demonstrated that the AP-4–FHF interaction reflects direct binding between the AP-4 μ 4 subunit and the Hook1 and Hook2 subunits of the FHF complex. These analyses further showed that these interactions are mediated by the C-terminal domain of AP-4 μ 4 and the CC1 and CC2 domains of Hook1. The formation of Hook1-Hook3 heterodimers discussed in the above paragraph is the likely explanation for the pull down of all three Hook proteins by AP-4 (Figure 2A) despite AP-4 μ 4 only binding to Hook1 and Hook2 (Figure 3, A and C).

The C-terminus of AP-4 μ 4 was previously shown to mediate recognition of tyrosine-based YXX Φ E-type signals in the cytosolic tail of transmembrane cargo proteins (Burgos *et al.*, 2010), including ATG9A (Mattera *et al.*, 2017). However, the C-terminal region of AP μ subunits and the μ homology domains (μ HD) of related proteins such as the stonins and the muniscins Fcho1/Fcho2 also recognize sequences or domains other than tyrosine-based signals in either transmembrane or cytosolic proteins. For example, basic residue motifs mediate binding of the cytosolic tails of synaptotagmin 1 (Haucke *et al.*, 2000), AMPA-type glutamate receptors (Kastning *et al.*, 2007), and GABA_A receptor subunits (Kittler *et al.*, 2005) to AP-2 μ 2 and synaptotagmin 1 to stonin 2 (Martina *et al.*, 2001; Maritzen *et al.*, 2010). A basic motif within the synaptotagmin 1 C2B domain also mediates binding to AP-2 μ 2 dependent on multimerization of the C2B domain (Grass *et al.*, 2004). Other examples are the binding of AP-2 μ 2 to stonin2 WxxF motifs (Walther *et al.*, 2004) and the dishevelled2 DEP domain (Yu *et al.*, 2010) and of Fcho1/Fcho2 to DPF motifs in Eps15 and Eps15R (Ma *et al.*, 2016). Our results thus extend the function of μ HDs to the recognition of CC domains in proteins lacking transmembrane domains. Further studies will be required to address the exact mode of recognition of the CC1 and CC2 domains in Hook1/Hook2 by AP-4- μ 4, whether this recognition depends on the dimerization of the CC region and

whether the AP-4 binding site for the YXX Φ E motif overlaps with that for Hook1/Hook2. In any event, our findings identify an AP-4 accessory factor that interacts with the μ 4 subunit rather than the hinge-ear domains of the ϵ and β 4 subunits, as is the case for tepsin (Borner *et al.*, 2012; Mattera *et al.*, 2015; Frazier *et al.*, 2016) and for most accessory factors that bind to hinge-ear domains of other AP complexes.

At this time, we do not know whether binding of AP-4 μ 4 to Hook1 and Hook2 may affect the function of these proteins as dynein–dynactin activating adaptors. The structural information available suggests that the Hook CC1-3 domains are important for high velocity and long run dynein–dynactin motility (Olenick *et al.*, 2016; Schroeder and Vale, 2016). It is then tempting to speculate that AP-4 μ 4 binding to the CC1 and CC2 domains of Hook1 and Hook2 homodimers or Hook1-Hook3 heterodimers may modulate the effect of these adaptors on the processivity of the dynein–dynactin complex. This possibility is reminiscent of the transition from autoinhibited to active state in another family of dynein adaptors, Bicaudal D, which is regulated by cargo binding to its CC regions (Liu *et al.*, 2013; Terawaki *et al.*, 2015; Huynh and Vale, 2017; McClintock *et al.*, 2018; Sladewski *et al.*, 2018; reviewed by Olenick and Holzbaur, 2019). Future studies should address whether AP-4 binding provides another regulatory layer modulating the ability of Hook proteins to activate the dynein–dynactin complex.

The C-terminal domain of Hook proteins is considered the cargo recognition dock, either directly or through interactions with other FHF subunits, in current models of transport driven by Hook–dynein–dynactin complexes (Reck-Peterson *et al.*, 2018; Dwivedi *et al.*, 2019b; Olenick and Holzbaur, 2019). The observations in the present study suggest a possible modification of this concept: that cargo may also be conveyed to the retrograde MT-based motor by an AP complex interacting with the CC domains of a dynein activating adaptor.

Role of the AP-4–FHF interaction in the cellular distribution of AP-4 and ATG9A

Combined silencing of all three Hook proteins or of FHIP or FHIP-L resulted in a more peripheral distribution of AP-4 and its cargo ATG9A, a phenotype similar to that caused by overexpression of the p150^{glued} dynactin subunit CC1 domain. The dispersal of AP-4 and ATG9A was more pronounced than that of TGN46, indicating that it did not just correspond to the population of AP-4 and ATG9A at the TGN. This dispersal was thus likely caused by uncoupling of AP-4- and ATG9A-containing vesicles from dynein–dynactin, with consequent inhibition of their retrograde transport toward the cell center (Figure 10). We think that this role of FHF counters that of another AP-4 interactor, the RUN-domain-containing accessory protein, RUSC2, which promotes anterograde transport of ATG9A vesicles toward the cell periphery, most likely by coupling the vesicles to kinesin motor proteins (Davies *et al.*, 2018) (Figure 10). As is the case for other intracellular organelles, the ability of AP-4/ATG9A vesicles to move in both anterograde and retrograde directions may be essential for the distribution of their functions through the entire cytoplasm.

Delivery of ATG9A to preautophagosomal structures is essential for the formation and expansion of autophagosomes (Orsi *et al.*, 2012; Zavodszky *et al.*, 2013), and its inhibition in AP-4-knockout cells results in impaired conversion of LC3B-I to LC3B-II (Mattera *et al.*, 2017; Davies *et al.*, 2018; De Pace *et al.*, 2018; Ivankovic *et al.*, 2020). KD of FHF subunits, however, did not affect LC3B-I to LC3B-II conversion or overall levels of LC3B in cells. The only noticeable effects were changes in the morphology

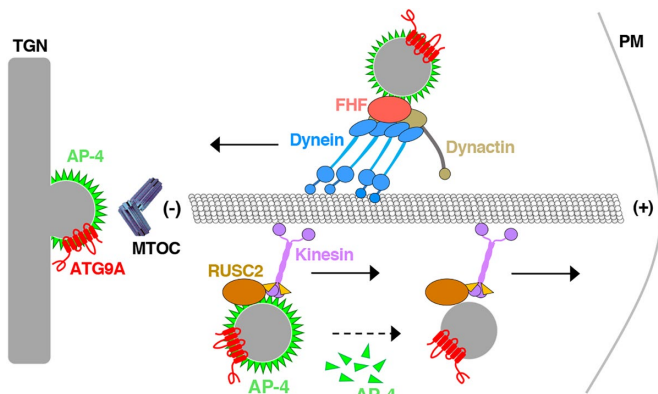


FIGURE 10: Proposed model for the MT-dependent transport of ATG9A-containing vesicles. AP-4- and ATG9A-containing vesicles are shown to undergo retrograde transport from the periphery to the center of the cell by virtue of coupling to dynein–dynactin via the FHF complex (this study) and anterograde transport from the center to the periphery of the cell by coupling to kinesin via the RUN and SH3 domain-containing protein 2 (RUSC2) (Davies *et al.*, 2018). This proposed role of the FHF complex is based on the interaction of AP-4 with subunits of the FHF complex (Figures 1–4), the colocalization of AP-4 with FHF subunits (Figure 5), and the effects of silencing of FHF subunits on localization of AP-4 and ATG9A reported in this study (Figures 6–8). The FHF complex is shown to interact with AP-4 (this study), with cytoplasmic dynein (through binding of the HD of Hook proteins to the C-terminus of dynein LIC subunits) and to dynactin (resulting in stabilization of dynein–dynactin complex by coiled-coil domains of Hook proteins) (for review, see Dwivedi *et al.*, 2019b). Two dimeric dynein complexes bound to dynactin–FHF are shown based on recent cryo-EM structural studies of Hook3–dynein–dynactin complexes (Grotjahn *et al.*, 2018; Urnavicius *et al.*, 2018). RUSC2 and kinesin are shown to remain associated with ATG9A vesicles after dissociation of AP-4, as reported by Davies *et al.* (2018). Coupling of AP-4- and ATG9A-containing vesicles to dynein–dynactin and kinesin allows distribution of these vesicles to different regions of the cell. FHF: fused toes protein homolog (FTS)/Hook/FTS- and Hook-interacting protein (FHIP) complex; MTOC: MT organizing center.

of LC3B-containing autophagosomes in a small fraction of FHIP- and FHIP-L-KD cells. These findings suggest that dispersal of ATG9A to the cell periphery, as seen in FHF-deficient cells, is less consequential for autophagy than its accumulation at the TGN, as observed in AP-4-deficient cells. The apparent lack of an effect of ATG9A dispersal on autophagy could be due to the cell type used in our study; perhaps effects could be seen in other cell types such as neurons. For example, the effects of AP-4 deficiency and retention of ATG9A in the TGN were more manifest in neurons, as evidenced by the impaired clearance of pathological protein aggregates in the axon of AP-4-KO mice (De Pace *et al.*, 2018; Ivankovic *et al.*, 2020). Underscoring the importance of the FHF complex in the brain, reduced levels of Hook1 and Hook3 were found in brain tissue of patients with Alzheimer’s disease, and silencing of Hook3 was shown to enhance β -amyloid production (Herrmann *et al.*, 2015). Hook2 was also found to regulate the formation of aggresomes (Szebenyi *et al.*, 2007), juxtannuclear structures that accumulate misfolded proteins targeted for autophagy (Garcia-Mata *et al.*, 2002). This could be due to a role of Hook proteins in coupling of autophagosomes to dynein–dynactin (Ravikumar *et al.*, 2005; Kimura *et al.*, 2008; Maday *et al.*, 2012; Reck-Peterson *et al.*, 2018). In light of our findings, however, some of the effects of Hook perturbations on autophagy could be due to its role in coupling ATG9A vesicles to dynein–dynactin.

MATERIALS AND METHODS

Recombinant DNA constructs

The human AP-4 ϵ and human tepsin constructs tagged at their N-terminus with a TSF epitope (pcDNA 3.1-TSF-AP-4- ϵ and pcDNA 3.1-TSF-tepsin) were described previously (Mattera *et al.*, 2015). The pcDNA 3.1-TSF-myrylsin (BORC subunit LOH12CR1) construct was described by Pu *et al.* (2015). The human Hook1, Hook2, and Hook3 constructs in pCMV-GST (pDEST27) and MSCV-N-HA/FLAG-human FTS (Xu *et al.*, 2008) were a gift from J. Wade Harper (Harvard Medical School). The human Hook1, Hook2, Hook3, and FTS cDNAs were PCR-amplified and subcloned into the pGBT9 and pGADT7 vectors (Clontech). The pGBT9-FHIP (isoform 2 with 972 residues) was previously described (Guo *et al.*, 2016). This FHIP construct was also subcloned in pGADT7. The cDNA encoding full-length human FHIP-L (*FAM160A1* gene product) was PCR-amplified from a human brain library (Clontech) and subsequently subcloned into pGBT9 and pGADT7. The human AP-4 ϵ , β_4 , and σ_4 constructs subcloned into pGADT7 (Boehm *et al.*, 2001) and mouse AP-1 μ_1A , human AP-1 μ_1B , mouse AP-2 μ_2 , rat AP-3 μ_3A , rat AP-3 μ_3B , and human AP-4 μ_4 constructs subcloned into pACT2 (Clontech) (Guo *et al.*, 2013) were previously described. A cDNA fragment encoding human AP-4 μ_4 followed by a GSGSGSGSGSG spacer and an HA tag was excised from the pCl-neo- μ_4 -GSGSGSGSGSG-(HA)₃ construct (Mattera *et al.*, 2014) and ligated into pGBT9. A stop codon was subsequently introduced at the end of the μ_4 coding sequence in order to generate pGBT9-human AP-4 μ_4 . The pGBT9-human tepsin and pGBT9-rat TGN38 tail construct (residues 324–353) were previously described (Mattera *et al.*, 2015). Sequences encoding human AP-4 ϵ fused to GST, TSF-tagged human AP-4 β_4 fused to maltose-binding protein, and human AP-4 μ_4 and human AP-4 σ_4 were cloned into pCAG-based vectors. Mutations were generated by site-directed mutagenesis and confirmed by DNA sequencing.

Antibodies

The following antibodies were used in this study: rabbit anti-Hook-1 (1:2,000 for IB; 1:1,000 for IF), rabbit anti-Hook2 (1:500 for IB, 1:750 for IF), and rabbit anti-Hook3 (1:2,000 for IB; 1:1,500 for IF) were gifts from Helmut Krämer (University of Texas Southwestern Medical Center); rabbit anti-FHIP (Abcam cat. ab184160, 1:1,000 for IB); mouse anti-AP-4 ϵ (BD Biosciences cat. 612028, 1:400 for IB, 1:75 for IF); rabbit anti-AP-4 β_4 (C-terminus) generated in our laboratory (anti-AP-4 β_4C in Dell’Angelica *et al.*, 1999; 1: 500 for IB; also used for IP); mouse anti-FLAG epitope (Sigma cat. F3165, 1:1,000 for IF); mouse anti-GFP (Roche cat. 11814460001, used for IP); mouse anti- α -tubulin (Sigma cat. T9026, 1:2,000 for IB); rabbit anti-ATG9A (Abcam cat. ab108338, 1:200 for IF); rabbit anti-LC3B (Cell Signaling cat. 3868S, 1:200 for IF); rabbit anti-LC3B (Sigma cat. L7543, 1:1,000 for IB); sheep anti-TGN46 (Bio-Rad cat. AHP500G, 1:1,000 for IF); Alexa Fluor 488–conjugated donkey anti-mouse IgG (ThermoFisher cat. A-21202, 1:1,000 for IF); Alexa Fluor 488–conjugated donkey anti-rabbit IgG (ThermoFisher cat. A-21206, 1:1,000 for IF); Alexa Fluor 555–conjugated donkey anti-mouse IgG (ThermoFisher cat. A-31570, 1:1,000 for IF); Alexa Fluor 555–conjugated donkey anti-rabbit IgG (ThermoFisher cat. A-31572, 1:1,000 for IF); Alexa Fluor 647–conjugated donkey anti-sheep IgG (ThermoFisher cat. A-21448, 1:1,000 for IF); HRP–conjugated sheep anti-mouse IgG (GE Healthcare cat. NXA931, 1:5,000 for IB); HRP–conjugated donkey anti-rabbit IgG (GE Healthcare cat. NA934V, 1:5,000 for IB).

TAP–MS analysis

The identification of copurifying proteins by TAP–MS of lysates from H4 human neuroglioma cells stably transfected with TSF-tagged

human AP-4 ϵ or TSF-tagged human tepsin was performed as described previously (Mattera *et al.*, 2015).

Cell culture and transfection protocols

H4 human neuroglioma cells, HeLa, and HEK293T cells were obtained from ATCC. H4 cells stably transfected with TSF-tagged human AP-4 ϵ or TSF-tagged human tepsin, HEK293T, and HeLa cells were grown in Dulbecco's modified Eagle's medium containing 4.5 g/l glucose and supplemented with 10% fetal bovine serum, 2 mM L-glutamine, and 100 U/ml penicillin–streptomycin (all reagents from ThermoFisher) at 37°C in a 5% CO₂ atmosphere. Cells were intermittently grown in culture medium supplemented with MycoZap Prophylactic (Lonza) to prevent mycoplasma contamination. Cells plated on 100-mm dishes were transfected with 7 μ g per of plasmid DNA using 27 μ l of X-tremeGENE 9 reagent (Roche) in 500 μ l of Opti-MEM I (ThermoFisher). Cells seeded on 6-well plates were cotransfected with a total of 1.4 μ g of total plasmid DNA per well (0.35 μ g of each of the four constructs encoding AP-4 subunits) using 5.4 μ l of X-tremeGENE 9 reagent in 100 μ l of Opti-MEM I.

Pull down and co-IP experiments

Experiments were performed in either transiently transfected HEK293T cells or H4 human neuroglioma cells stably transfected with TSF-tagged human AP-4 ϵ . Cells plated on 100-mm dishes were lysed in 0.8 ml of 50 mM Tris-HCl, pH 7.4, 0.8% (vol/vol) Triton X-100, and 75 mM NaCl supplemented with protease inhibitors (EDTA-free Complete, Roche). Following a 30-min incubation with rotation at 4°C, extracts were centrifuged for 15 min at 21,000 \times g and 4°C and the supernatants were subjected to IB, pull down, or IP. Pull down of TSF-tagged constructs from lysates with Strep-Tactin beads (IBA) was performed as described (Mattera *et al.*, 2015). IP of lysates was performed as previously described (Mattera *et al.*, 2003) using 2.5 μ g of antibodies immobilized on 25 μ l of Protein G-Sepharose beads (GE Healthcare).

Pulled-down or immunoprecipitated complexes were subjected to SDS-PAGE on 10% acrylamide gels and transferred to Immobilon-P membranes (Millipore). Blots were incubated with the indicated primary and HRP-conjugated secondary antibodies and developed by enhanced chemiluminescence using Western Lighting Plus-ECL (PerkinElmer), SuperSignal West Pico Plus, or SuperSignal West Femto reagents (ThermoFisher).

Y2H assays

Assays were carried out using the Gal4-based Matchmaker system and the AH109 reporter yeast strain as previously described (Mattera *et al.*, 2003).

RNA interference

ON-TARGETplus SMART pool siRNAs aimed at the following human targets were purchased from Dharmacon (catalogue number followed by target): L-021474-00-0005, AP-4 ϵ ; L-011918-01-0005, AP-4 μ 4; L-016845-01-0005, Hook1; L-020408-02-0005, Hook2; L-013558-01-0005, Hook3; L-014783-02-0005, FHIP (FAM160A2 gene product); L-184739-00-0005, FHIP-L (FAM160A1 gene product). A nontargeting siRNA (cat. D-001810-01-05) was used as control. Cells were seeded on 6-well plates and subjected to two rounds of transfection at times 0 and 48 h with 200 nM siRNAs using the Oligofectamine reagent (ThermoFisher) at a 4 μ l/ml concentration. Triple silencing of Hook proteins was carried out at a total siRNA concentration of 480 nM and 7–8 μ l/ml Oligofectamine. Cells were split and replated 48–72 h after the second round of treatment and analyzed by IB and IF on the next day.

Amino acid, serum starvation, and bafilomycin treatment

Control and siRNA-treated cells were seeded on 12-well plates the day before the experiment. For amino acid and serum starvation, cells were washed twice with 1 ml of phosphate-buffered saline (PBS) at 37°C followed by the addition of 1 ml of amino acid-free DMEM (MyBioSource) supplemented with 3.7 g/l sodium bicarbonate and 3.5 g/l glucose (final concentration of glucose was 4.5 g/l). Cells were incubated for 45 min at 37°C in a 5% CO₂ atmosphere. Incubations were stopped by removal of medium followed by washing with 1 ml of PBS at 37°C and lysis in 0.15–0.2 ml of 1 \times Laemmli buffer. Lysates were incubated for 10 min at 90°C followed by centrifugation for 2 min at 16,000 \times g and room temperature. Supernatants were analyzed by SDS-PAGE (12% acrylamide gels) and IB for LC3B and α -tubulin. Control and siRNA-treated cells seeded on 12-well plates were also incubated for 4 h at 37°C in a 5% CO₂ atmosphere in the presence or absence of 100 nM bafilomycin A1 (Sigma) added to the regular culture medium. Cells were subsequently washed with PBS and lysed in Laemmli buffer, and the extracts were analyzed by SDS-PAGE and IB as described in the preceding paragraph.

Quantitative real-time RT-PCR

Total RNA from HeLa cells treated with nontargeting siRNA (control) or ON-TARGETplus SMART pool siRNA targeting FHIP-L was prepared using the RNeasy Mini kit (Qiagen) following the manufacturer's instructions. Samples containing 250 ng of total RNA were reverse transcribed using the Super Script VILO cDNA synthesis kit (Invitrogen). Levels of reverse-transcribed mRNA encoding FHIP-L were quantified using TaqMan gene expression assays (ThermoFisher) with FAM-probe/primer Hs04935393_m1 for FAM160A1 (encoding FHIP-L) along with VIC-probe/primers Hs01060665-g1 for ACTB (β -actin) as reference gene. PCR amplification was performed on triplicate cDNA samples originated from 15 ng of total RNA using TaqMan Fast Advanced Master Mix (ThermoFisher) and monitored in an AriaMX Real-Time PCR system (Agilent Technologies). Absolute expression levels were calculated from calibration curves obtained with serial dilutions of pGBT9-FHIP-L (10⁻³ to 10⁻⁷ μ g/ml range). Relative expression was calculated using the 2^{- $\Delta\Delta$ CT} method (Livak and Schmittgen, 2001), where Δ CT is the difference in threshold cycles (CT) between the target (FHIP-L) and the reference gene transcripts (β -actin) and $\Delta\Delta$ CT is the difference in Δ CT between the silenced (FHIP-L KD) and the control sample.

IF microscopy

Cells were fixed for 10 min in –20°C methanol and incubated with the indicated dilutions of primary (45–60 min at room temperature) and secondary antibodies (30–45 min at room temperature) in 0.1% bovine serum albumin, 0.1% saponin, and 0.02% sodium azide in PBS. DAPI (ThermoFisher) at 1:2,000 dilution and GFP-Booster Atto488 (Chromotek) at 1:400 dilution were added during incubation with secondary antibodies to stain nuclei and GFP constructs in transfected cells, respectively. Relative dispersal of AP-4 ϵ and ATG9A signals following treatment with siRNA pools or transfection with GFP-p150-CC1 was assessed by manual scoring of cells using a Zeiss Axio Imager.A1 fluorescence microscope (Plan Apochromat 63 \times /1.4 Oil DIC M27 objective) and by calculation of Spearman's rank correlation values (next paragraph). Confocal microscopy images were obtained using Zeiss LSM 780 (63 \times /1.4 NA Plan Apochromat 63 \times objective) or Zeiss 880 (63 \times /1.4 NA Plan Apochromat 63 \times objective) laser scanning confocal microscopes.

Image analysis

Colocalization analysis was carried out using the Pearson–Spearman correlation plugin for ImageJ (French *et al.*, 2008). Scatter plots of colocalization report the Spearman's rank correlation value *r*, representing the relationship of the signal intensity from green and red channels of analyzed images. This value can range from -1 to $+1$, where 0 indicates no relationship, and -1 and $+1$ indicate a perfectly negative or positive correlation, respectively. The closer the *r* value is to $+1$, the more likely is the colocalization of signals. The plugin allows masking of areas to be included in the analysis. In a given image, TGN46-positive Golgi structures were masked prior to analysis using the selection brush tool as described (French *et al.*, 2008). A threshold level of 10 was set, under which pixel values were considered noise and not included in the statistical analysis. Statistical significance was analyzed by one-way ANOVA followed by two-tailed Dunnett's test using GraphPad Prism (GraphPad Software).

ACKNOWLEDGMENTS

We thank Helmut Krämer (University of Texas Southwestern Medical Center) and J. Wade Harper (Harvard Medical School) for kind gifts of reagents, and Amra Saric for advice on quantitative real-time RT-PCR. This work was supported by the Intramural Program of NICHD, NIH (ZIA HD001607 to JSB) and by NIH grant R01 AI120691 to XR.

REFERENCES

- Abdollahpour H, Alawi M, Kortüm F, Beckstette M, Seemanova E, Komárek V, Rosenberger G, Kutsche K (2015). An AP4B1 frameshift mutation in siblings with intellectual disability and spastic tetraplegia further delineates the AP-4 deficiency syndrome. *Eur J Hum Genet* 23, 256–259.
- Abou Jamra R, Philippe O, Raas-Rothschild A, Eck SH, Graf E, Buchert R, Borck G, Ekici A, Brockschmidt FF, Nöthen MM, *et al.* (2011). Adaptor protein complex 4 deficiency causes severe autosomal-recessive intellectual disability, progressive spastic paraplegia, shy character, and short stature. *Am J Hum Genet* 88, 788–795.
- Baron Gaillard CL, Pallesi-Pocachard E, Massey-Harroche D, Richard F, Arsanto JP, Chauvin JP, Lecine P, Krämer H, Borg JP, Le Bivic A (2011). Hook2 is involved in the morphogenesis of the primary cilium. *Mol Biol Cell* 22, 4549–4562.
- Bauer P, Leshinsky-Silver E, Blumkin L, Schlipf N, Schröder C, Schicks J, Lev D, Riess O, Lerman-Sagie T, Schöls L (2012). Mutation in the AP4B1 gene cause hereditary spastic paraplegia type 47 (SPG47). *Neurogenetics* 13, 73–76.
- Bielska E, Schuster M, Roger Y, Berepiki A, Soanes DM, Talbot NJ, Steinberg G (2014). Hook is an adapter that coordinates kinesin-3 and dynein cargo attachment on early endosomes. *J Cell Biol* 204, 989–1007.
- Boehm M, Aguilar RC, Bonifacino JS (2001). Functional and physical interactions of the adaptor protein complex AP-4 with ADP-ribosylation factors (ARFs). *EMBO J* 20, 6265–6276.
- Borner GH, Antrobus R, Hirst J, Bhumbra GS, Kozik P, Jackson LP, Sahlender DA, Robinson MS (2012). Multivariate proteomic profiling identifies novel accessory proteins of coated vesicles. *J Cell Biol* 197, 141–160.
- Burgos PV, Mardones GA, Rojas AL, DaSilva LL, Prabhu Y, Hurley JH, Bonifacino JS (2010). Sorting of the Alzheimer's disease amyloid precursor protein mediated by the AP-4 complex. *Dev Cell* 18, 425–436.
- Davies AK, Itzhak DN, Edgar JR, Archuleta TL, Hirst J, Jackson LP, Robinson MS, Borner GHH (2018). AP-4 vesicles contribute to spatial control of autophagy via RUSC-dependent peripheral delivery of ATG9A. *Nat Commun* 9, 3958.
- Dell'Angelica EC, Mullins C, Bonifacino JS (1999). AP-4, a novel protein complex related to clathrin adaptors. *J Biol Chem* 274, 7278–7285.
- De Pace R, Skirzewski M, Damme M, Mattera R, Mercurio J, Foster AM, Cuitino L, Jarnik M, Hoffmann V, Morris HD, *et al.* (2018). Altered distribution of ATG9A and accumulation of axonal aggregates in neurons from a mouse model of AP-4 deficiency syndrome. *PLoS Genet* 14, e1007363.
- Dwivedi D, Kumari A, Rathi S, Mylavaram SVS, Sharma M (2019a). The dynein adaptor Hook2 plays essential roles in mitotic progression and cytokinesis. *J Cell Biol* 218, 871–894.
- Dwivedi D, Chawla P, Sharma M (2019b). Incorporating motility in the motor: role of the hook protein family in regulating dynein motility. *Biochemistry* 58, 1026–1031.
- Ebrahimi-Fakhari D, Cheng C, Dies K, Diplock A, Pier DB, Ryan CS, Lanpher BC, Hirst J, Chung WK, Sahin M, *et al.*, CureSPG47 (2018). Clinical and genetic characterization of AP4B1-associated SPG47. *Am J Med Genet A* 176, 311–318.
- Frazier MN, Davies AK, Voehler M, Kendall AK, Borner GH, Chazin WJ, Robinson MS, Jackson LP (2016). Molecular basis for the interaction between AP4 β 4 and its accessory protein, tepsin. *Traffic* 17, 400–415.
- French AP, Mills S, Swarup R, Bennett MJ, Pridmore TP (2008). Colocalization of fluorescent markers in confocal microscope images of plant cells. *Nat Protoc* 3, 619–628.
- Gama JB, Pereira C, Simões PA, Celestino R, Reis RM, Barbosa DJ, Pires HR, Carvalho C, Amorim J, Carvalho AX, *et al.* (2017). Molecular mechanism of dynein recruitment to kinetochores by the Rod-Zw10-Zwlich complex and Spindly. *J Cell Biol* 216, 943–960.
- Garcia-Mata R, Gao YS, Sztul E (2002). Hassles with taking out the garbage: aggravating aggregates. *Traffic* 3, 388–396.
- Grass I, Thiel S, Höning S, Haucke V (2004). Recognition of a basic AP-2 binding motif within the C2B domain of synaptotagmin is dependent on multimerization. *J Biol Chem* 279, 54872–54880.
- Grotjahn DA, Chowdhury S, Xu Y, McKenney RJ, Schroer TA, Lander GC (2018). Cryo-electron tomography reveals that dynactin recruits a team of dyneins for processive motility. *Nat Struct Mol Biol* 25, 203–207.
- Guardia CM, De Pace R, Mattera R, Bonifacino JS (2018). Neuronal functions of adaptor complexes involved in protein sorting. *Curr Opin Neurobiol* 51, 103–110.
- Guo X, Fariás GG, Mattera R, Bonifacino JS (2016). Rab5 and its effector FHF contribute to neuronal polarity through dynein-dependent retrieval of somatodendritic proteins from the axon. *Proc Natl Acad Sci USA* 113, E5318–E5327.
- Guo X, Mattera R, Ren X, Chen Y, Retamal C, González A, Bonifacino JS (2013). The adaptor protein-1 μ 1B subunit expands the repertoire of basolateral sorting signal recognition in epithelial cells. *Dev Cell* 27, 353–366.
- Hardies K, May P, Djémié T, Tarta-Arsene O, Deconinck T, Craui D; AR working group of the EuroEPINOMICS RES Consortium; Helbig I, Suls A, Balling R, Weckhuysen S, *et al.* (2015). Recessive loss-of-function mutations in AP4S1 cause mild fever-sensitive seizures, developmental delay and spastic paraplegia through loss of AP-4 complex assembly. *Hum Mol Genet* 24, 2218–2227.
- Haucke V, Wenk MR, Chapman ER, Farsad K, De Camilli P (2000). Dual interaction of synaptotagmin with μ 2- and α -adaptin facilitates clathrin-coated pit nucleation. *EMBO J* 19, 6011–6019.
- Herrmann L, Wiegmann C, Arsalan-Werner A, Hilbrich I, Jäger C, Flach K, Suttkus A, Lachmann I, Arendt T, Holzer M (2015). Hook proteins: association with Alzheimer pathology and regulatory role of hook3 in amyloid beta generation. *PLoS One* 10, e0119423.
- Hirst J, Bright NA, Rous B, Robinson MS (1999). Characterization of a fourth adaptor-related protein complex. *Mol Biol Cell* 10, 2787–2802.
- Hirst J, Schlacht A, Norcott JP, Traynor D, Bloomfield G, Antrobus R, Kay RR, Dacks JB, Robinson MS (2014). Characterization of TSET, an ancient and widespread membrane trafficking complex. *Elife* 3, e02866.
- Hurley JH, Lee S, Prag G (2006). Ubiquitin-binding domains. *Biochem J* 399, 361–372.
- Huttlin EL, Bruckner RJ, Paulo JA, Cannon JR, Ting L, Baltier K, Colby G, Gebreab F, Gygi MP, Parzen H, *et al.* (2017). Architecture of the human interactome defines protein communities and disease networks. *Nature* 545, 505–509.
- Huynh W, Vale RD (2017). Disease-associated mutations in human BICD2 hyperactivate motility of dynein-dynactin. *J Cell Biol* 216, 3051–3060.
- Ivankovic D, Drew J, Lesept F, White IJ, López Doménech G, Tooze SA, Kittler JT (2020). Axonal autophagosome maturation defect through failure of ATG9A sorting underpins pathology in AP-4 deficiency syndrome. *Autophagy* 16, 391–407.
- Kabeya Y, Mizushima N, Yamamoto A, Oshitani-Okamoto S, Ohsumi Y, Yoshimori T (2004). LC3, GABARAP and GATE16 localize to autophagosomal membrane depending on form-II formation. *J Cell Sci* 117, 2805–2812.
- Kastning K, Kukhtina V, Kittler JT, Chen G, Pechstein A, Enders S, Lee SH, Sheng M, Yan Z, Haucke V (2007). Molecular determinants for the interaction between AMPA receptors and the clathrin adaptor complex AP-2. *Proc Natl Acad Sci USA* 104, 2991–2996.
- Kendrick AA, Dickey AM, Redwine WB, Tran PT, Vaites LP, Dzieciatkowska M, Harper JW, Reck-Peterson SL (2019). Hook3 is a scaffold for the opposite-polarity microtubule-based motors cytoplasmic dynein-1 and KIF1C. *J Cell Biol* 218, 2982–3001.

- Kimura S, Noda T, Yoshimori T (2008). Dynein-dependent movement of autophagosomes mediates efficient encounters with lysosomes. *Cell Struct Funct* 33, 109–122.
- Kittler JT, Chen G, Honing S, Bogdanov Y, McAnish K, Arancibia-Carcamo IL, Jovanovic JN, Pangalos MN, Haucke V, Yan Z, Moss SJ (2005). Phospho-dependent binding of the clathrin AP2 adaptor complex to GABAA receptors regulates the efficacy of inhibitory synaptic transmission. *Proc Natl Acad Sci USA* 102, 14871–14876.
- Krämer H, Phistry M (1996). Mutations in the *Drosophila* hook gene inhibit endocytosis of the boss transmembrane ligand into multivesicular bodies. *J Cell Biol* 133, 1205–1215.
- Krämer H, Phistry M (1999). Genetic analysis of hook, a gene required for endocytic trafficking in *Drosophila*. *Genetics* 151, 675–684.
- Lee IG, Olenick MA, Boczkowska M, Franzini-Armstrong C, Holzbaur ELF, Dominguez R (2018). A conserved interaction of the dynein light intermediate chain with dynein-dynactin effectors necessary for processivity. *Nat Commun* 9, 986.
- Lesche R, Peetz A, van der Hoeven F, Rütger U (1997). Ft1, a novel gene related to ubiquitin-conjugating enzymes, is deleted in the Fused toes mouse mutation. *Mamm Genome* 8, 879–883.
- Liu Y, Salter HK, Holding AN, Johnson CM, Stephens E, Lukavsky PJ, Walshaw J, Bullock SL (2013). Bicaudal-D uses a parallel, homodimeric coiled coil with heterotypic registry to coordinate recruitment of cargos to dynein. *Genes Dev* 27, 1233–1246.
- Livak KJ, Schmittgen TD (2001). Analysis of relative gene expression data using real-time quantitative PCR and the 2(-Delta Delta C(T)) Method. *Methods* 25, 402–408.
- Ma L, Umasankar PK, Wrobel AG, Lyman A, McCoy AJ, Holkar SS, Jha A, Pradhan-Sundt T, Watkins SC, Owen DJ, Traub LM (2016). Transient Fcho1/2-Eps15/R-AP-2 nanoclusters prime the AP-2 clathrin adaptor for cargo binding. *Dev Cell* 37, 428–44.
- Maday S, Wallace KE, Holzbaur EL (2012). Autophagosomes initiate distally and mature during transport toward the cell soma in primary neurons. *J Cell Biol* 196, 407–417.
- Maldonado-Báez L, Cole NB, Krämer H, Donaldson JG (2013). Microtubule-dependent endosomal sorting of clathrin-independent cargo by Hook1. *J Cell Biol* 201, 233–247.
- Maritzen T, Podufall J, Haucke V (2010). Stonins—specialized adaptors for synaptic vesicle recycling and beyond? *Traffic* 11, 8–15.
- Martina JA, Bonangelino CJ, Aguilar RC, Bonifacino JS (2001). Stonin 2: an adaptor-like protein that interacts with components of the endocytic machinery. *J Cell Biol* 153, 1111–1120.
- Mattera R, Arighi CN, Lodge R, Zerial M, Bonifacino JS (2003). Divalent interaction of the GGAs with the Rabaptin-5-Rabex-5 complex. *EMBO J* 22, 78–88.
- Mattera R, Boehm M, Chaudhuri R, Prabhu Y, Bonifacino JS (2011). Conservation and diversification of dileucine signal recognition by adaptor protein (AP) complex variants. *J Biol Chem* 286, 2022–2030.
- Mattera R, Farias GG, Mardones GA, Bonifacino JS (2014). Co-assembly of viral envelope glycoproteins regulates their polarized sorting in neurons. *PLoS Pathog* 10, e1004107.
- Mattera R, Guardia CM, Sidhu SS, Bonifacino JS (2015). Bivalent motif-ear interactions mediate the association of the accessory protein tepsin with the AP-4 adaptor complex. *J Biol Chem* 290, 30736–30749.
- Mattera R, Park SY, De Pace R, Guardia CM, Bonifacino JS (2017). AP-4 mediates export of ATG9A from the trans-Golgi network to promote autophagosome formation. *Proc Natl Acad Sci USA* 114, E10697–E10706.
- McClintock MA, Dix CI, Johnson CM, McLaughlin SH, Maizels RJ, Hoang HT, Bullock SL (2018). RNA-directed activation of cytoplasmic dynein-1 in reconstituted transport RNPs. *Elife* 7, e36312.
- McKenney RJ, Huynh W, Tanenbaum ME, Bhabha G, Vale RD (2014). Activation of cytoplasmic dynein motility by dynactin-cargo adapter complexes. *Science* 345, 337–341.
- Mellacheruvu D, Wright Z, Couzens AL, Lambert JP, St-Denis NA, Li T, Miteva YV, Hauri S, Sardi ME, Low TY, et al. (2013). The CRAPome: a contaminant repository for affinity purification-mass spectrometry data. *Nat Methods* 10, 730–736.
- Moreno-De-Luca A, Helmers SL, Mao H, Burns TG, Melton AM, Schmidt KR, Fernhoff PM, Ledbetter DH, Martin CL (2011). Adaptor protein complex-4 (AP-4) deficiency causes a novel autosomal recessive cerebral palsy syndrome with microcephaly and intellectual disability. *J Med Genet* 48, 141–144.
- Olenick MA, Dominguez R, Holzbaur ELF (2019). Dynein activator Hook1 is required for trafficking of BDNF-signaling endosomes in neurons. *J Cell Biol* 218, 220–233.
- Olenick MA, Holzbaur ELF (2019). Dynein activators and adaptors at a glance. *J Cell Sci* 132, jcs227132.
- Olenick MA, Tokito M, Boczkowska M, Dominguez R, Holzbaur EL (2016). Hook adaptors induce unidirectional processive motility by enhancing the dynein-dynactin interaction. *J Biol Chem* 291, 18239–18251.
- Orsi A, Razi M, Dooley HC, Robinson D, Weston AE, Collinson LM, Tooze SA (2012). Dynamic and transient interactions of Atg9 with autophagosomes, but not membrane integration, are required for autophagy. *Mol Biol Cell* 23, 1860–1873.
- Pu J, Schindler C, Jia R, Jarnik M, Backlund P, Bonifacino JS (2015). BIRC, a multisubunit complex that regulates lysosome positioning. *Dev Cell* 33, 176–188.
- Qiu R, Zhang J, Xiang X (2018). p25 of the dynactin complex plays a dual role in cargo binding and dynactin regulation. *J Biol Chem* 293, 15606–15619.
- Quintyne NJ, Gill SR, Eckley DM, Crego CL, Compton DA, Schroer TA (1999). Dynactin is required for microtubule anchoring at centrosomes. *J Cell Biol* 147, 321–334.
- Ravikumar B, Acevedo-Arozena A, Imarisio S, Berger Z, Vacher C, O’Kane CJ, Brown SD, Rubinsztein DC (2005). Dynein mutations impair autophagic clearance of aggregate-prone proteins. *Nat Genet* 37, 771–776.
- Reck-Peterson SL, Redwine WB, Vale RD, Carter AP (2018). The cytoplasmic dynein transport machinery and its many cargoes. *Nat Rev Mol Cell Biol* 19, 382–398.
- Redwine WB, DeSantis ME, Hollyer I, Htet ZM, Tran PT, Swanson SK, Florens L, Washburn MP, Reck-Peterson SL (2017). The human cytoplasmic dynein interactome reveals novel activators of motility. *Elife* 6, e28257.
- Robinson MS (2004). Adaptable adaptors for coated vesicles. *Trends Cell Biol* 14, 167–174.
- Robinson MS (2015). Forty years of clathrin-coated vesicles. *Traffic* 16, 1210–1238.
- Schroeder CM, Vale RD (2016). Assembly and activation of dynein-dynactin by the cargo adaptor protein Hook3. *J Cell Biol* 214, 309–318.
- Siddiqui N, Zwetsloot AJ, Bachmann A, Roth D, Hussain H, Brandt J, Kaverina I, Straube A (2019). PTPN21 and Hook3 relieve KIF1C autoinhibition and activate intracellular transport. *Nat Commun* 10, 2693.
- Sladewski TE, Billington N, Ali MY, Bookwalter CS, Lu H, Kremntsova EB, Schroer TA, Trybus KM (2018). Recruitment of two dyneins to an mRNA-dependent Bicaudal D transport complex. *Elife* 7, e36306.
- Szebenyi G, Wigley WC, Hall B, Didier A, Yu M, Thomas P, Krämer H (2007). Hook2 contributes to aggresome formation. *BMC Cell Biol* 8, 19.
- Terawaki S, Yoshikane A, Higuchi Y, Wakamatsu K (2015). Structural basis for cargo binding and autoinhibition of Bicaudal-D1 by a parallel coiled-coil with homotypic registry. *Biochem Biophys Res Commun* 460, 451–456.
- Tesson C, Koht J, Stevanin G (2015). Delving into the complexity of hereditary spastic paraplegias: how unexpected phenotypes and inheritance modes are revolutionizing their nosology. *Hum Genet* 134, 511–538.
- Traub LM, Bonifacino JS (2013). Cargo recognition in clathrin-mediated endocytosis. *Cold Spring Harb Perspect Biol* 5, a016790.
- Tüysüz B, Bilguvar K, Koçer N, Yalçınkaya C, Çağlayan O, Gül E, Sahin S, Çomu S, Günel M (2014). Autosomal recessive spastic tetraplegia caused by AP4M1 and AP4B1 gene mutation: expansion of the facial and neuroimaging features. *Am J Med Genet A* 164A, 1677–1685.
- Urnavicius L, Lau CK, Elshenawy MM, Morales-Rios E, Motz C, Yildiz A, Carter AP (2018). Cryo-EM shows how dynactin recruits two dyneins for faster movement. *Nature* 554, 202–206.
- Verkerk AJ, Schot R, Dumeé B, Schellekens K, Swagemakers S, Bertoli-Avella AM, Lequin MH, Dudink J, Govaert P, van Zwol AL, et al. (2009). Mutation in the AP4M1 gene provides a model for neuroaxonal injury in cerebral palsy. *Am J Hum Genet* 85, 40–52.
- Walenta JH, Didier AJ, Liu X, Krämer H (2001). The Golgi-associated hook3 protein is a member of a novel family of microtubule-binding proteins. *J Cell Biol* 152, 923–934.
- Walther K, Diril MK, Jung N, Haucke V (2004). Functional dissection of the interactions of stonin 2 with the adaptor complex AP-2 and synaptotagmin. *Proc Natl Acad Sci USA* 101, 964–969.
- Xiang X, Qiu R, Yao X, Arst HN Jr, Peñalva MA, Zhang J (2015). Cytoplasmic dynein and early endosome transport. *Cell Mol Life Sci* 72, 3267–3280.
- Xu L, Sowa ME, Chen J, Li X, Gygi SP, Harper JW (2008). An FTS/Hook/p107(FHIP) complex interacts with and promotes endosomal clustering by the homotypic vacuolar protein sorting complex. *Mol Biol Cell* 19, 5059–5071.
- Yamaguchi J, Suzuki C, Nanao T, Kakuta S, Ozawa K, Tanida I, Saitoh T, Sunabori T, Komatsu M, Tanaka K, et al. (2018). Atg9a deficiency causes

- axon-specific lesions including neuronal circuit dysgenesis. *Autophagy* 14, 764–777.
- Yao X, Wang X, Xiang X (2014). FHIP and FTS proteins are critical for dynein-mediated transport of early endosomes in *Aspergillus*. *Mol Biol Cell* 25, 2181–2189.
- Yap CC, Murate M, Kishigami S, Muto Y, Kishida H, Hashikawa T, Yano R (2003). Adaptor protein complex-4 (AP-4) is expressed in the central nervous system neurons and interacts with glutamate receptor delta2. *Mol Cell Neurosci* 24, 283–295.
- Yu A, Xing Y, Harrison SC, Kirchhausen T (2010). Structural analysis of the interaction between Dishevelled2 and clathrin AP-2 adaptor, a critical step in noncanonical Wnt signaling. *Structure* 18, 1311–1320.
- Zavodszky E, Vicinanza M, Rubinsztein DC (2013). Biology and trafficking of ATG9 and ATG16L1, two proteins that regulate autophagosome formation. *FEBS Lett* 587, 1988–1996.
- Zhang J, Qiu R, Arst HN Jr, Peñalva MA, Xiang X (2014). HookA is a novel dynein-early endosome linker critical for cargo movement in vivo. *J Cell Biol* 204, 1009–1026.